

---

# Scattering of anti-plane waves by scalene trapezoidal boundary with embedded cavity in anisotropic material based on mapping space

Yingchao Sun<sup>1,2</sup>, Yuliang Li<sup>2</sup>, Haibin Lin<sup>2</sup>, Zailin Yang<sup>1,3\*</sup>

<sup>1</sup> *College of Aerospace and Civil Engineering, Harbin Engineering University, Harbin, China*

<sup>2</sup> *AVIC-HONGDU, Nanchang, China*

<sup>3</sup> *Key Laboratory of Advanced Material of Ship and Mechanics, Ministry of Industry and Information Technology, Harbin*

accepted date      ; received date      ; in original form date

running head: Dynamic response of hill and a tunnel in anisotropic medium

Corresponding author: Zailin Yang

Phone: +8619917629545

E-mail: yangzailin00@163.com

---

# Scattering of anti-plane waves by scalene trapezoidal boundary with embedded cavity in anisotropic material based on mapping space

Yingchao Sun<sup>1,2</sup>, Zailin Yang<sup>1,3\*</sup>, Yuliang Li<sup>2</sup>, Haibin Lin<sup>2</sup>

<sup>1</sup> College of Aerospace and Civil Engineering, Harbin Engineering University, Harbin, China

<sup>2</sup> AVIC-HONGDU, Nanchang, China

<sup>3</sup>Key Laboratory of Advanced Material of Ship and Mechanics, Ministry of Industry and Information Technology, Harbin

## Abstract

Both surface motion and hole stress concentration have always been concerned in anisotropic medium. In this paper, a theoretical approach is used to study the scattering problem of circular holes under a scalene trapezoid on the surface. The mapping function that anisotropic medium to homogeneous medium is established, and the relationship between the free boundary of anisotropic medium and the mapping of homogeneous medium boundary is proved. In the space of homogeneous medium mapping, the wave displacement function is obtained by solving the equation of motion that meets the zero-stress boundary conditions by separating the variable method and the symmetric method. Based on the complex function, multi-polar coordinate method and region-matching technique, algebraic equations are established at auxiliary boundary and free boundary conditions in complex domain. Then according to sample statistics, least square method is used instead of the Fourier expansion method to solve the undetermined coefficient of the algebraic equations by discrete boundary. Numerical results shows that the continuity of the auxiliary boundary and the accuracy of the zero-stress boundary are nice, and the displacement of the free surface and the stress of the circular hole are related to the parameters of material medium, the position of the circular hole, the direction of the incident wave and the frequency content of the excitation. Finally the process of the wave propagation and scattering around trapezoid and shallow circle are shown in time domain through the inverse fourier transform.

**Keywords:** *Surface motion; anisotropic material; mapping function; SH-wave scattering; least square method; complex function; Region-matching technique; half-space*

## 1. Introduction

Dynamic response of non-linear boundary in anisotropic medium has always been an important research topic in the field of wave motion. It is helpful for the research on inverse problems of the elastic wave, and it is meaningful for the site survey and prospecting, seismic research, underwater

---

detection and target identification, large-scale wall vibration analysis, nondestructive testing, flaw detection, etc. Pioneering work in this area was done in early 1970s. The wave function expansion method was used to analyze the local semi-cylindrical canyon scattering in the half space under the action of incident SH waves<sup>1,2</sup>. Hermite function and mapping function was applied to analyze scattering of SH waves with arbitrary shape depressions<sup>3</sup>. Subsequently, the Graf's addition theorem provided an analytical solution to the SH waves scattering by a cylindrical canyon of circular-arc cross-section<sup>4</sup>, and weighted residual method was applied to 2D canyons of arbitrary shape<sup>5</sup>. The degenerate kernels and Fourier series expansions were adopted in the null-field integral equation to analyze the surface motion of multiple alluvial valleys for incident plane SH waves<sup>6</sup>.

Due to the multiple reflections of the incident wave on the convex surface, the scattering of the incident wave by the convex surface is more complicated than that on the concave surface. The two-dimensional model was divided into a closed circular region and a half space with a semi-circular concave topography by introducing a semi-circular auxiliary boundary, to study the scattering of plane SH waves by a semi-cylindrical hill in the half-space<sup>7-10</sup>. In fact Region-matching technique was used to study more complex boundary which the entire wavefield solution in each individual region is well defined and well behaved since it satisfies the governing equation and all boundary conditions except at the fictitious interface. Such as V-shaped canyon, circular sectorial canyon, deep semi-elliptic canyon with a horizontal edge<sup>11-16</sup>. Application of complex displacement fields, mapping method, series expansion and mirror image method to solve scattering of waves in complex structure<sup>17-21</sup>. Such as the anti-plane response of an isosceles trapezoid, an scalene trapezoid, an isosceles trapezoidal hill to SH waves<sup>22-24</sup>. In addition, numerical methods are also used to solve the scattering of SH waves by concave and convex topography. Hybrid method based on combination of transfinite interpolation and series expansion solves the problem of irregular surface scattering<sup>25</sup>. A hybrid method based on the combination of lamb series and finite element method was also used to investigate a dike with trapezoidal structure and a circular-arc foundation embedded in an elastic half-space<sup>26</sup>. In recent years, new methods have also emerged to solve the wave problem, such as the refined dynamic theory, the partial differential operator theory.

In engineering, some materials need to be simplified into gradient material models or anisotropic material models. Due to the large number of independent constants in non-uniform media, the scattering field of elastic waves becomes more complicated. For example, the propagation of gradient material waves was studied<sup>27-31</sup>, and the complex wave function method was used to give a solution of SH-wave scattering in circular holes, depressions, and cylindrical semicircular sedimentary valleys in anisotropic media<sup>32-39</sup>. Boundary element method was used to study the scattering of SH waves by holes and inclusions in an anisotropic body and an anisotropic

---

elastic layer in infinite domain<sup>40-43</sup>. In addition, numerical methods were also used to study cross-anisotropic material<sup>44,45</sup>.

In this paper based on the existing research results, the SH wave scattering problem of shallow circular hole under scalene trapezoid in anisotropic medium is studied. A more flexible non-semicircle region division method is used to solve the shallow hole problem, and use auxiliary circle to solve singularity of reflex angle at trapezoid corner which singularity was proposed by Achenbach<sup>46</sup>. The mapping function from anisotropic medium to homogeneous medium is derived, and revise the transformation function of professor Diankui Liu<sup>32,33</sup>. The relationship between the free boundary of anisotropic medium and the boundary of mapped homogeneous medium is proved, and the wave displacement function is obtained by solving the wave equation that meets the scalene trapezoid zero-stress boundary conditions by separating the variable method in the mapped homogeneous medium space. The wave function that satisfies the boundary conditions of the half-space is derived by using symmetry and complex coordinates in the mapping of the uniform medium space. The defect of directly constructing the half-space scattering wave function in the literature which doesn't consider anisotropic material asymmetry is corrected. Especially for the difference range of wave function series, and multiple auxiliary boundary continuous conditions, a more effective least square method which only need discrete boundary is proposed. The discrete point spacing and the boundary equation amplitude adjusting are used to coordinate Euclidean distance weight. After numerical simulation, the high accuracy of the auxiliary boundary continuity and the zero boundary condition prove the correctness of region-matching technique, wave function equation and least square method. Finally, the effects of different angles of incidence, the frequency content of the excitation, parameters of material medium, and positions of hole on surface motion and hole stress are discussed in frequency domain, and the process of the wave propagation and scattering around trapezoid and shallow circle are shown in time domain. For many years, The mapping function from anisotropic medium to homogeneous medium and the function of constructing the half-space scattering wave are given. At the same time. the singularity of reflex angle and wave function which satisfy anisotropic medium wedge free edge are solved.

## **2. Methodology**

### *2.1 Model*

The model consists of a scalene trapezoid on half space and a hole under free surface shown in Fig 1 a). SH-wave propagates in anisotropic half space with modulus  $C_{44}$   $C_{45}$   $C_{55}$  and density  $\rho$  at incident angle  $\alpha$ .  $C_1$  and  $C_2$  symbolize trapezoidal waist with the gradients of 1:n<sub>1</sub> and 1:n<sub>2</sub>,  $C_3$  is trapezoidal upper flat surface, and S represent half space free flat surface.

In order to solve singularity of reflex angle at trapezoid corner, and obtain the global displacement function which satisfy equation (1) and complicated boundary conditions, use region-matching technique and auxiliary circle. (a) The half space can be divided to region ① ② ③ ④ ⑤ and ⑥ by auxiliary boundary  $D_1 D_2 D_3 D_4 D_5 D_6$  with circle center  $O_1 O_2 O_3 O_4 O_5 O_8$ .  $P_1 P_2 P_3$  and  $P_4$  are the projection of  $O_1 O_2 O_3 O_4 O_5 O_8$  on the flat surface. Auxiliary circle  $D_4$  and  $D_5$  are used to solve singularity of reflex angle at trapezoid corner  $O_4$  and  $O_5$ . (b)  $O_3$  is the intersection of the extension lines of the  $C_1$  and mid-perpendicular of the  $X_4X_5$ , where  $X_4, X_5$  are the intersection point of circle  $D_4, D_5$  and the trapezoidal edge respectively. (c)  $O$  is the intersection of the extension lines of the trapezoid side  $C_1$  and  $C_2$ . Local coordinate systems are established as shown in the figure. Once the radius of  $D_4$  and  $D_5$  are given, all dimensions of each radius can be determined by the graphical relationship. Usually the radius of  $r_4$  and  $r_5$  are smaller. Each angle is presented in Appendix A for details.

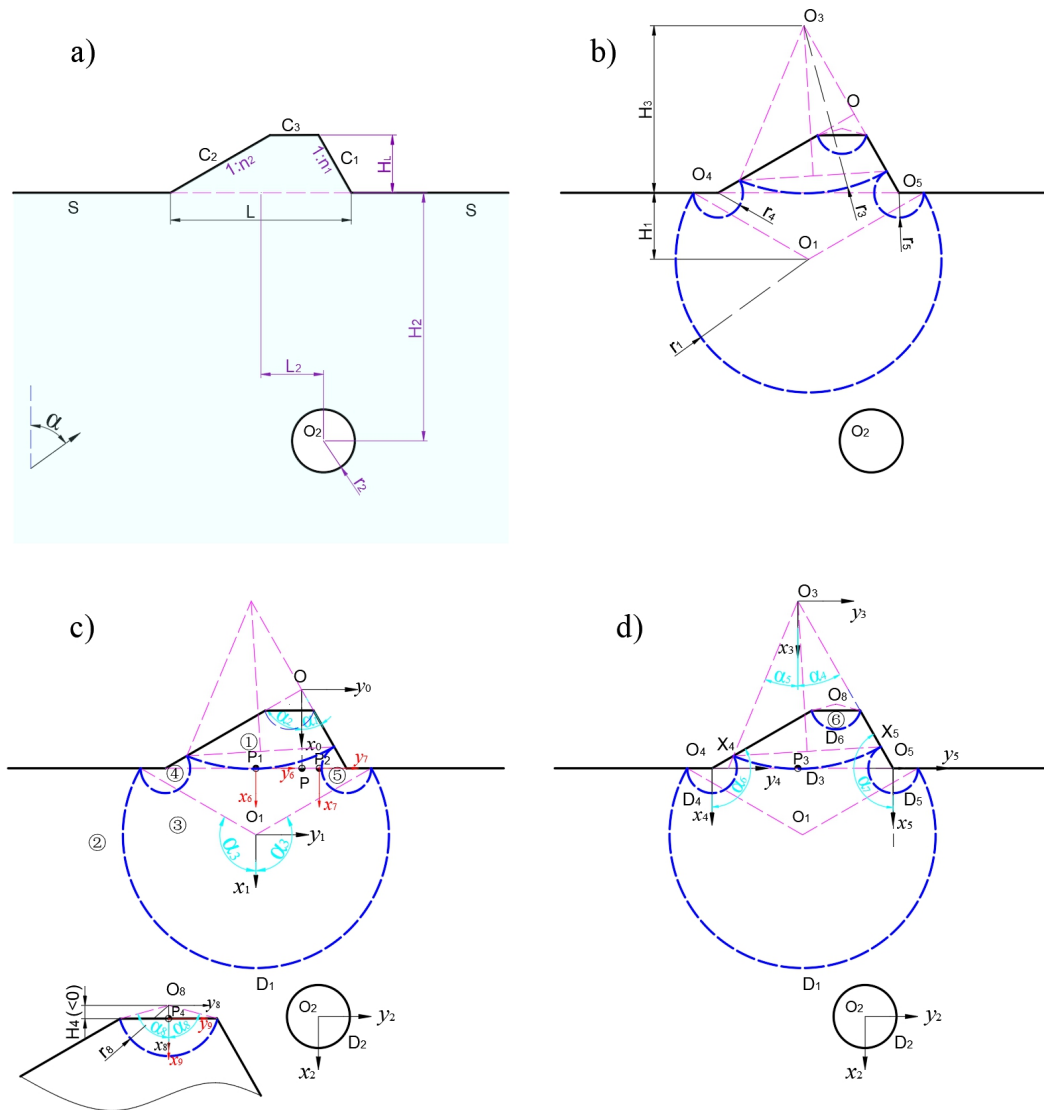


Fig 1. The model of the scalene trapezoid with a hole and regions divided

## 2.2 Equation of motion and mapping function

From the stress-strain relationship in an anisotropic medium, the SH wave equation is

$$C_{55} \frac{\partial^2 w}{\partial x^2} + 2C_{45} \frac{\partial^2 w}{\partial x \partial y} + C_{44} \frac{\partial^2 w}{\partial y^2} = \rho \frac{\partial^2 w}{\partial t^2} \quad (1)$$

Introducing complex variables  $z = x + yi$  and  $\bar{z} = x - yi$ , in the complex plane  $(z, \bar{z})$ , Eq.(1) can be rewritten as:

$$(C_{55} - C_{44} + 2C_{45}i) \frac{\partial^2 w}{\partial z^2} + 2(C_{44} + C_{55}) \frac{\partial^2 w}{\partial z \partial \bar{z}} + (C_{55} - C_{44} - 2C_{45}i) \frac{\partial^2 w}{\partial \bar{z}^2} = \rho \frac{\partial^2 w}{\partial t^2} \quad (2)$$

Correspondingly, radial stress and hoop stress have the forms of

$$\tau_{rz} = \frac{1}{2} \left\{ \left[ (C_{55} + C_{44}) \frac{\partial w}{\partial z} + (C_{55} - C_{44} - 2C_{45}i) \frac{\partial w}{\partial \bar{z}} \right] e^{\theta i} + \left[ (C_{55} - C_{44} + 2C_{45}i) \frac{\partial w}{\partial z} + (C_{55} + C_{44}) \frac{\partial w}{\partial \bar{z}} \right] e^{-\theta i} \right\} \quad (3)$$

$$\tau_{\theta z} = \frac{1}{2} \left\{ \left[ (C_{55}i + C_{44}i) \frac{\partial w}{\partial z} + (C_{55}i - C_{44}i + 2C_{45}) \frac{\partial w}{\partial \bar{z}} \right] e^{\theta i} + \left[ (-C_{55}i + C_{44}i + 2C_{45}) \frac{\partial w}{\partial z} + (-C_{55}i - C_{44}i) \frac{\partial w}{\partial \bar{z}} \right] e^{-\theta i} \right\} \quad (4)$$

In order to convert the left side of the above formula (2) into a form  $\partial^2 w / \partial \chi \partial \bar{\chi}$ , the following conversion is performed

$$\frac{\partial^2 w}{\partial \chi \partial \bar{\chi}} = \left( \frac{\partial z}{\partial \chi} \frac{\partial \bar{z}}{\partial \bar{\chi}} \right) \frac{\partial^2 w}{\partial z^2} + \left( \frac{\partial \bar{z}}{\partial \chi} \frac{\partial z}{\partial \bar{\chi}} + \frac{\partial z}{\partial \chi} \frac{\partial \bar{z}}{\partial \bar{\chi}} \right) \frac{\partial^2 w}{\partial z \partial \bar{z}} + \left( \frac{\partial \bar{z}}{\partial \chi} \frac{\partial \bar{z}}{\partial \bar{\chi}} \right) \frac{\partial^2 w}{\partial \bar{z}^2} + \frac{\partial w}{\partial z} \left( \frac{\partial^2 z}{\partial \bar{\chi} \partial \chi} \right) + \frac{\partial w}{\partial \bar{z}} \left( \frac{\partial^2 \bar{z}}{\partial \bar{\chi} \partial \chi} \right) \quad (5)$$

Comparing formula (2) and formula (5), get:

$$\begin{cases} \frac{\partial z}{\partial \chi} \frac{\partial \bar{z}}{\partial \bar{\chi}} = C_{55} - C_{44} + 2C_{45}i & (a) \\ \frac{\partial \bar{z}}{\partial \chi} \frac{\partial z}{\partial \bar{\chi}} + \frac{\partial z}{\partial \chi} \frac{\partial \bar{z}}{\partial \bar{\chi}} = 2(C_{44} + C_{55}) & (b) \\ \frac{\partial \bar{z}}{\partial \chi} \frac{\partial \bar{z}}{\partial \bar{\chi}} = C_{55} - C_{44} - 2C_{45}i & (c) \\ \frac{\partial^2 z}{\partial \bar{\chi} \partial \chi} = \frac{\partial^2 \bar{z}}{\partial \bar{\chi} \partial \chi} = 0 & (d) \end{cases} \quad (6)$$

From item (d), the solution form of z is:

$$z = a\chi + b\bar{\chi} + c \quad (7)$$

Set special solution  $c = 0$ , from (a), (b), (c), know that there are three unknown real numbers in z, let  $a = \hat{x} + \hat{y}i, b = \hat{x} + \hat{z}i$  or  $a = \hat{x} + \hat{z}i, b = \hat{y} + \hat{z}i$ , substitute z into items (a), (b), (c) can obtain

$$\begin{cases} a = \frac{C_{45} + \left( C_{44} \pm \sqrt{C_{44}C_{55} - C_{45}^2} \right) i}{\sqrt{C_{44}}} \\ b = \frac{C_{45} + \left( C_{44} \mp \sqrt{C_{44}C_{55} - C_{45}^2} \right) i}{\sqrt{C_{44}}} \end{cases} \quad \text{or} \quad \begin{cases} a = \frac{C_{55} \pm \sqrt{C_{44}C_{55} - C_{45}^2} + C_{45}i}{\sqrt{C_{55}}} \\ b = \frac{C_{55} \mp \sqrt{C_{44}C_{55} - C_{45}^2} + C_{45}i}{\sqrt{C_{55}}} \end{cases}$$

$\chi \bar{\chi}$  is expressed as

$$\begin{cases} \chi = \frac{b\bar{z} - \bar{a}z}{b\bar{b} - a\bar{a}} \\ \bar{\chi} = \frac{\bar{b}z - a\bar{z}}{b\bar{b} - a\bar{a}} \end{cases} \quad (8)$$

Comparing the above four results, know that: the second solution (a) term takes a positive sign in homogeneous medium,  $\chi = z, \bar{\chi} = \bar{z}$ . so this solution is taken for convenience. Of course other solutions are also correct.

In order to convert into form  $4u \frac{\partial^2 w}{\partial \xi \partial \bar{\xi}} = \rho \frac{\partial^2 w}{\partial t^2}$ ,  $a$  and  $b$  are expressed by dimensionless  $\gamma_1, \gamma_2$  and equivalent elastic modulus  $\mu$

$$\begin{cases} \xi = \frac{1}{2}(\bar{\gamma}_1 z - \gamma_2 \bar{z}) \\ \bar{\xi} = \frac{1}{2}(\gamma_1 \bar{z} - \bar{\gamma}_2 z) \end{cases} \quad (9)$$

$$\text{Where } \begin{cases} \gamma_1 = \frac{C_{55} + \sqrt{C_{44}C_{55} - C_{45}^2} + C_{45}i}{C_{55}} \\ \gamma_2 = \frac{C_{55} - \sqrt{C_{44}C_{55} - C_{45}^2} + C_{45}i}{C_{55}} \end{cases}, \text{ and } \mu = (C_{44}C_{55} - C_{45}^2)/C_{55}$$

For the convenience of expression, this paper defines a mapping function  $\xi = \xi(z)$  to represent complex conversion. The above formula (1) is transformed into

$$4 \frac{\partial^2 w}{\partial \xi \partial \bar{\xi}} = \frac{1}{c_T^2} \frac{\partial^2 w}{\partial t^2} \quad (10)$$

Where  $c_T^2 = \frac{\mu}{\rho}$ . After separating the time variables, the above formula becomes

$$\frac{\partial^2 w}{\partial \xi \partial \bar{\xi}} = \left(\frac{ik}{2}\right)^2 w \quad (11)$$

Where  $k = \omega/c_T$ . Then the solution of the above formula (11) scattered wave is

$$w(\xi, \bar{\xi}) = \sum_{n=-\infty}^{+\infty} A_n H_n^1(k|\xi|) \left(\frac{\xi}{|\xi|}\right)^n \quad (12)$$

Correspondingly, radial stress and hoop stress have the forms of

$$\begin{aligned} \tau_{rz} &= \left( f_1^r \frac{\partial w}{\partial \xi} + f_2^r \frac{\partial w}{\partial \bar{\xi}} \right) e^{\theta i} + \left( f_3^r \frac{\partial w}{\partial \xi} + f_4^r \frac{\partial w}{\partial \bar{\xi}} \right) e^{-\theta i} \\ \tau_{\theta z} &= \left( f_1^\theta \frac{\partial w}{\partial \xi} + f_2^\theta \frac{\partial w}{\partial \bar{\xi}} \right) e^{\theta i} + \left( f_3^\theta \frac{\partial w}{\partial \xi} + f_4^\theta \frac{\partial w}{\partial \bar{\xi}} \right) e^{-\theta i} \end{aligned} \quad (13)$$

Where  $f_1^r, f_2^r, f_3^r, f_4^r, f_1^\theta, f_2^\theta, f_3^\theta, f_4^\theta$  presented in Appendix.

Establish a cartesian coordinate system  $(x',y')$ , which is defined as  $\xi = x' + y'i, \bar{\xi} = x' - y'i$ .

According to literature <sup>3</sup>, this coordinate system  $(x',y')$  is a homogeneous medium mapping coordinate system correspond to an anisotropic medium coordinate system  $(x,y)$ . It is known from equation (9) that the complex modulus  $|\zeta|$  is related to the complex  $z$  phase angle  $\theta$  and modulus  $|z|$ , and the complex  $\zeta$  phase angle  $\theta'$  is only related to the  $z$  phase angle  $\theta$ . Suppose the functional relationship is  $\theta' = f(\theta) = \text{angle}(\zeta(z))$ .

### 2.3 Wave function in region ①

In the trapezoidal region ①, the total waves consist of the scattered waves  $W^{D6(1)}$  and standing wave  $W^{D3(1)}$  by the auxiliary boundary  $D_6$  and  $D_3$ , it need satisfy governing Eq. (2) and free hypotenuse condition.

Zero-stress condition of free surface hypotenuse  $C_1$  and  $C_2$  in region ① at the coordinate system  $(x,y)$  can be expressed as:

$$\tau_{\theta_0 z}^c = \begin{cases} 0 & \theta_0 = \alpha_1 \\ 0 & \theta_0 = \alpha_2 \end{cases} \quad (14)$$

In cartesian coordinate system  $(x_0, y_0)$  and  $(x_0', y_0')$ , the boundary stress is expressed as

$$\begin{cases} \tau_{\theta_0 z} = (f_1^\theta e^{\theta i} + f_3^\theta e^{-\theta i}) \frac{\partial w}{\partial \xi} + (f_2^\theta e^{\theta i} + f_4^\theta e^{-\theta i}) \frac{\partial w}{\partial \bar{\xi}} & (a) \\ \tau_{\theta_0 z} = \frac{2i\mu'}{r'} \left( \zeta \frac{\partial w}{\partial \zeta} - \bar{\zeta} \frac{\partial w}{\partial \bar{\zeta}} \right) = \frac{ir\mu'}{r'} \left( (\bar{\gamma}_1 e^{\theta i} - \gamma_2 e^{-\theta i}) \frac{\partial w}{\partial \zeta} - (\gamma_1 e^{-\theta i} - \bar{\gamma}_2 e^{\theta i}) \frac{\partial w}{\partial \bar{\zeta}} \right) & (b) \end{cases} \quad (15)$$

It is known that the hypotenuse of the triangle in the mapping space is also a straight line from the functional relationship  $\theta' = f(\theta) = \text{angle}(\zeta(z))$ . Substituting the boundary condition (14) into item (a) of the above formula (15), get

$$\frac{\partial w / \partial \xi}{\partial w / \partial \bar{\xi}} = - \frac{(f_2^\theta e^{\theta i} + f_4^\theta e^{-\theta i})}{(f_1^\theta e^{\theta i} + f_3^\theta e^{-\theta i})} \quad (16)$$

Substituting the above formula (16) into the term (b), the boundary stress in the coordinate system  $(x_0', y_0')$  is obtained

$$\tau_{\theta_0 z}^c = \begin{cases} 0 & \theta'_0 = f(\alpha_1) \\ 0 & \theta'_0 = f(\alpha_2) \end{cases} \quad (17)$$

The coordinate system  $(x_e', y_e')$  is established which the  $x_e'$ -axis bisects the angle of the triangle corner in mapping space. The governing equation of the polar coordinate system  $(r_e', \theta_e')$  corresponding to the coordinates  $(x_e', y_e')$  is

$$\frac{1}{r_e'} \frac{\partial}{\partial r} \left( r_e' \frac{\partial w}{\partial r_e'} \right) + \frac{1}{r_e'^2} \frac{\partial^2 w}{\partial \theta_e'^2} + k^2 w = 0 \quad (18)$$

Solving the wave equation that satisfies the boundary conditions using the separation variable method is:

$$w = \sum A_{\lambda_1} J_{\lambda_1}(kr'_e) \cos(\lambda_1 \theta'_e) + B_{\lambda_2} J_{\lambda_2}(kr'_e) \sin(\lambda_2 \theta'_e) \quad (19)$$

$$\text{Where } \lambda_1 = \frac{2m\pi}{f(\alpha_1) - f(\alpha_2)} \text{ or } \lambda_2 = \frac{(2m+1)\pi}{f(\alpha_1) - f(\alpha_2)} \quad m = 0, 1, 2 \dots$$

On the complex plane  $(\xi_e, \bar{\xi}_e)$  corresponding to the coordinate system  $(x_e', y_e')$ , the standing wave function of the above formula (19) is written as

$$W^{D3(1)}(\xi_e, \bar{\xi}_e) = W_0 \sum_{m=0}^{+\infty} \left\{ C_m J_{mp_0}(K_1 |\xi_e|) \left[ \left( \frac{\xi_e}{|\xi_e|} \right)^{mp_0} + (-1)^m \left( \frac{\xi_e}{|\xi_e|} \right)^{-mp_0} \right] \right\} \quad (20)$$

Where  $W_0$  is the displacement amplitude, it is supposed to be unity in this paper.  $C_m$  is coefficient to be determined.  $J_{mp_0}()$  is Bessel function with  $mp_0$  th order.  $p_0 = \pi / (f(\alpha_1) - f(\alpha_2))$ .

According to moving coordinates from  $(x_e', y_e')$  to  $(x_0', y_0')$ ,  $\xi_0$  can be expressed as

$$\xi_e = \xi_0 e^{q_0 i} \quad (21)$$

Where  $q_0 = -(f(\alpha_1) + f(\alpha_2)) / 2$

Substituting (21) into equation (20) and returning to the coordinate system  $(x_0, y_0)$ , in the complex plane  $(Z_j, \bar{Z}_j)$ , equation (20) can be expressed as

$$W^{D3(1)}(Z_j, \bar{Z}_j) = W_0 \sum_{m=0}^{+\infty} \left\{ C_m J_{mp_0}(K_1 |\xi(Z_{0j}) e^{q_0 i}|) \left[ \left( \frac{\xi(Z_{0j}) e^{q_0 i}}{|\xi(Z_{0j}) e^{q_0 i}|} \right)^{mp_0} + (-1)^m \left( \frac{\xi(Z_{0j}) e^{q_0 i}}{|\xi(Z_{0j}) e^{q_0 i}|} \right)^{-mp_0} \right] \right\} \quad (22)$$

Where

$$Z_{0j} = \begin{cases} Z_3 + b_{03} & j = 3 \\ Z_8 + b_{08} & j = 8 \end{cases}$$

and  $b_{03} = H - H_3 + (H \tan(\alpha_1) - H_3 \tan(\alpha_4))i$  is the complex coordinates of  $O_3$  with origin at  $O$ .

$b_{08} = \frac{L}{n_1 + n_2} - H_L + H_4 + \frac{n_1 - n_2}{2} \left( \frac{L}{n_1 + n_2} - H_L \right) i$  is the complex coordinates of  $O_8$  with origin at  $O$ . In

$W^{D3(1)}$  characters, superscripts  $(1)$  means region ①, superscripts  $D3$  represent auxiliary boundary  $D3$ .

$K_1$  is the shear wave number of region ①. The following symbol marking method is similar.

The corresponding shear stresses are:

$$\tau_{r_j z}^{D3(1)}(Z_j, \bar{Z}_j) = \sum_{m=0}^{+\infty} C_m \hat{P}_{mp_0}^J(Z_{0j}) \quad (23)$$

$$\tau_{\theta_j z}^{D3(1)}(Z_j, \bar{Z}_j) = \sum_{m=0}^{+\infty} C_m \hat{Q}_{mp_0}^J(Z_{0j}) \quad (24)$$

Where  $\hat{P}_{mp}^J$ ,  $\hat{Q}_{mp}^J$  presented in Appendix, and  $H_j = 0$ .

Similarly, the scattered waves  $W^{D6(1)}$  can be rewritten as

$$W^{D6(1)}(Z_j, \bar{Z}_j) = W_0 \sum_{m=0}^{+\infty} \left\{ B_m \mathbf{H}_{mp_0}^1 \left( K_1 \left| \xi(Z_{0j}) e^{q_0 i} \right| \right) \left[ \left( \frac{\xi(Z_{0j}) e^{q_0 i}}{\left| \xi(Z_{0j}) e^{q_0 i} \right|} \right)^{mp_0} + (-1)^m \left( \frac{\xi(Z_{0j}) e^{q_0 i}}{\left| \xi(Z_{0j}) e^{q_0 i} \right|} \right)^{-mp_0} \right] \right\} \quad (25)$$

The corresponding shear stresses are:

$$\tau_{r_3 z}^{D6(1)}(Z_j, \bar{Z}_j) = \sum_{m=0}^{+\infty} \left\{ C_m \hat{P}_{mp_0}^{H^1}(Z_{0j}) \right\} \quad (26)$$

$$\tau_{\theta_3 z}^{D3(1)}(Z_j, \bar{Z}_j) = \sum_{m=0}^{+\infty} \left\{ C_m \hat{Q}_{mp_0}^{H^1}(Z_{0j}) \right\} \quad (27)$$

## 2.4 Wave function in region ②

In the opening region ②, the total waves can be split into incident waves  $W^{(i)}$ , reflected waves  $W^{(r)}$  from the horizontal free surface  $S$ , and the scattered waves  $W^{D1}$  and  $W^{D2}$  by the auxiliary boundary  $D_1$  and the hole edge  $D_2$ .

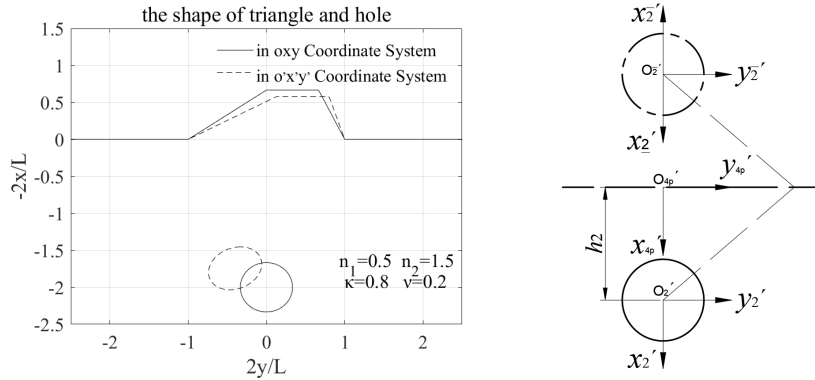


Fig 2. Circular hole symmetry in mapping space

Due to the anisotropy of the material, a semi-infinite space scattering field cannot be directly constructed by the symmetric method. So need to construct a solution with the help of the material homogeneity field of the mapping space. The surface stress is  $\tau_{\theta'_z}^S = 0$  from the Eq.(15), and material is isotropic in mapping space  $(x', y')$ . Based on complex coordinates and symmetric method, construct a semi-infinite space scattering field that satisfies boundary conditions according to symmetry. The scattering wave equation with two symmetrical holes is

$$w = \sum_{m=-\infty}^{+\infty} A_m \mathbf{H}_m^1(k |\xi_2(z)|) \left( \frac{\xi_2(z)}{|\xi_2(z)|} \right)^m + A_{m'} \mathbf{H}_{m'}^1(k |\xi_2(z)|) \left( \frac{\xi_2(z)}{|\xi_2(z)|} \right)^{m'} \quad (28)$$

By  $\xi_2 = \xi_2 - 2h_2$ ,  $\xi_2 = -\bar{\xi}_2$ ,  $\xi_2 = \xi_{4p} - h_2$ ,  $\xi_4 = \xi_{4p} - l_2$  relationship

$(h_2 = \text{real}(\xi(H_2)), l_2 = \text{imag}(\xi(H_2)) \times i)$  take into Eq.(28), it is expressed as follow

$$\begin{aligned}
w &= \sum_{m=-\infty}^{+\infty} A_m \mathbf{H}_m^1(k|\xi_2|) \left( \frac{\xi_2}{|\xi_2|} \right)^{m'} + A_m \mathbf{H}_m^1(k|\bar{\xi}_2 - 2h_2|) \left( \frac{-\bar{\xi}_2 - 2h_2}{|-\bar{\xi}_2 - 2h_2|} \right)^{m'} \\
&= \sum_{m=-\infty}^{+\infty} A_m \mathbf{H}_m^1(k|\xi_4 - \xi(H_2)|) \left( \frac{\xi_4 - \xi(H_2)}{|\xi_4 - \xi(H_2)|} \right)^{m'} + (-1)^m A_m \mathbf{H}_m^1(k|\xi_4 + \bar{\xi}(H_2)|) \left( \frac{\xi_4 + \bar{\xi}(H_2)}{|\xi_4 + \bar{\xi}(H_2)|} \right)^{-m'}
\end{aligned} \tag{29}$$

According to Eq.(29), equation of scattered wave  $W^{D2(2)}$  generated by boundary  $D_2$  and satisfying governing Eq. (2) and free boundary condition S in the complex plane  $(z_j, \bar{z}_j)$  can be written as

$$W^{D2(2)}(Z_j, \bar{Z}_j) = W_0 \sum_{m=-\infty}^{+\infty} \left\{ E_m \left[ \begin{aligned} &\mathbf{H}_m^1(K_2|\xi(Z_{7j}) - \xi(H_2)|) \left( \frac{\xi(Z_{7j}) - \xi(H_2)}{|\xi(Z_{7j}) - \xi(H_2)|} \right)^m + \\ &(-1)^m \mathbf{H}_m^1(K_2|\xi(Z_{7j}) + \bar{\xi}(H_2)|) \left( \frac{\xi(Z_{7j}) + \bar{\xi}(H_2)}{|\xi(Z_{7j}) + \bar{\xi}(H_2)|} \right)^{-m} \end{aligned} \right] \right\} \tag{30}$$

Where

$$Z_{7j} = \begin{cases} Z_1 + b_{71} & j = 1 \\ Z_2 + b_{72} & j = 2 \end{cases}$$

and  $b_{71} = H_1 - L_2i$ ,  $b_{72} = H_2$

Similarly, equation of scattered wave  $W^{D1(2)}$  generated by boundary  $D_1$  and satisfying governing Eq. (2) and free boundary condition S in the complex plane  $(z_j, \bar{z}_j)$  can be written as

$$W^{D1(2)}(Z_j, \bar{Z}_j) = W_0 \sum_{m=-\infty}^{+\infty} \left\{ D_m \left[ \begin{aligned} &\mathbf{H}_m^1(K_2|\xi(Z_{6j}) - \xi(H_1)|) \left( \frac{\xi(Z_{6j}) - \xi(H_1)}{|\xi(Z_{6j}) - \xi(H_1)|} \right)^m + \\ &(-1)^m \mathbf{H}_m^1(K_2|\xi(Z_{6j}) + \bar{\xi}(H_1)|) \left( \frac{\xi(Z_{6j}) + \bar{\xi}(H_1)}{|\xi(Z_{6j}) + \bar{\xi}(H_1)|} \right)^{-m} \end{aligned} \right] \right\} \tag{31}$$

Where

$$Z_{6j} = \begin{cases} Z_1 + b_{61} & j = 1 \\ Z_2 + b_{62} & j = 2 \end{cases}$$

and  $b_{61} = H_1$ ,  $b_{62} = H_2 + L_2i$

Above formula,  $W_0$  is the displacement amplitude.  $D_m$  and  $E_m$  are coefficient to be determined.

$\mathbf{H}_m^1()$  is Hankel function of first kind with  $m$ th order.

The corresponding shear stresses are:

$$\tau_{r_j z}^{D1(2)}(Z_j, \bar{Z}_j) = \sum_{m=-\infty}^{+\infty} D_m \hat{P}_m^{H^1}(Z_{6j}) \tag{32}$$

$$\tau_{\theta_j z}^{D1(2)}(Z_j, \bar{Z}_j) = \sum_{m=-\infty}^{+\infty} D_m \hat{Q}_m^{H^1}(Z_{6j}) \tag{33}$$

$$\tau_{rjz}^{D2(2)}(Z_j, \bar{Z}_j) = \sum_{m=-\infty}^{+\infty} E_m \hat{P}_m^{H^1}(Z_{7j}) \quad (34)$$

$$\tau_{\theta jz}^{D2(2)}(Z_j, \bar{Z}_j) = \sum_{m=-\infty}^{+\infty} E_m \hat{Q}_m^{H^1}(Z_{7j}) \quad (35)$$

In the above stress formula  $q=0$ , and see appendix for details.

Incident wave with incidence angle  $\alpha$ , can be represented in the cartesian coordinate system  $o_6x_6y_6$ <sup>32</sup>, and be written as

$$W^{(i)} = W_i e^{iK_2^i (y_6 \sin \alpha_i - x_6 \cos \alpha_i)} = W_i e^{\frac{-iK_2^i}{2} (z_6 e^{\alpha_i} + \bar{z}_6 e^{-\alpha_i})} \quad (36)$$

Where  $W_i = W_0$

Substituting into the wave equation (1), the wave velocity is:

$$c_{si} = \left\{ \left[ (\cos a_i)^2 C_{55} - (2 \sin a_i \cos a_i) C_{45} + (\sin a_i)^2 C_{44} \right] / \rho \right\}^{1/2}$$

Reflected wave can be written as

$$W^{(r)} = W_r e^{iK_2^r (y_6 \sin \alpha_r + x_6 \cos \alpha_r)} = W_r e^{\frac{iK_2^r}{2} (z_6 e^{-\alpha_r} + \bar{z}_6 e^{\alpha_r})} \quad (37)$$

Substituting into the wave equation (1), the wave velocity is:

$$c_{sr} = \left\{ \left[ (\cos a_r)^2 C_{55} + (2 \sin a_r \cos a_r) C_{45} + (\sin a_r)^2 C_{44} \right] / \rho \right\}^{1/2}$$

Substituting the total wave  $W = W^{(i)} + W^{(r)}$  into the free boundary zero stress condition  $\tau_{x_3 z_3}^S \Big|_{x_3=0} = 0$ ,

obtain

$$\begin{cases} \cot a_r = \cot a_i - 2C_{45}/C_{55} \\ W_r = W_i \\ K_2^r = K_2^i \sin \alpha_i / \sin \alpha_r \end{cases} \quad a_i \neq 0 \quad \text{or} \quad \begin{cases} a_r = a_i \\ W_r = W_i \\ K_2^r = K_2^i \end{cases} \quad a_i = 0$$

When  $\cot a_{r1} = \cot a_i - 2C_{45}/C_{55} \geq 0$ , the reflected wave is in the first quadrant; while  $\cot a_{r1} = \cot a_i - 2C_{45}/C_{55} < 0$  the reflected wave does not exist because the anisotropic medium changes the direction of wave propagation. It means that the incident angle  $\alpha_i$  can only be less than  $\text{acot}(2C_{45}/C_{55})$  near the surface. Its total expression is

$$W^{(i+r)}(Z_j, \bar{Z}_j) = W_0 e^{\frac{-iK_2^i}{2} (z_{6j} e^{\alpha_i} + \bar{z}_{6j} e^{-\alpha_i})} + W_0 e^{\frac{iK_2^r}{2} (z_{6j} e^{-\alpha_r} + \bar{z}_{6j} e^{\alpha_r})} \quad (38)$$

Substituting into Eq(3) and Eq(4), get the stress expression

$$\tau_{rjz}^{(i+r)}(Z_j, \bar{Z}_j) = \frac{1}{2} \left\{ \begin{aligned} & \left[ (C_{55} + C_{44})U(z_{6j}) + (C_{55} - C_{44} - 2C_{45}i)V(z_{6j}) \right] e^{\theta_i} + \\ & \left[ (C_{55} - C_{44} + 2C_{45}i)U(z_{6j}) + (C_{55} + C_{44})V(z_{6j}) \right] e^{-\theta_i} \end{aligned} \right\} \quad (39)$$

$$\tau_{\theta_j z}^{(i+r)}(Z_j, \bar{Z}_j) = \frac{1}{2} \left\{ \begin{aligned} & \left[ (C_{55}i + C_{44}i)U(z_{6j}) + (C_{55}i - C_{44}i + 2C_{45})V(z_{6j}) \right] e^{\theta_i} + \\ & \left[ (-C_{55}i + C_{44}i + 2C_{45})U(z_{6j}) + (-C_{55}i - C_{44}i)V(z_{6j}) \right] e^{-\theta_i} \end{aligned} \right\} \quad (40)$$

see appendix for details.

## 2.5 Wave function in region ③

In the enclosed region ③, the total waves are composed of  $W^{D1}$   $W^{D3}$   $W^{D4}$  and  $W^{D5}$  generated by the auxiliary boundary  $D_1$   $D_3$   $D_4$  and  $D_5$ . In the complex plane  $(z_j, \bar{z}_j)$ , it can be written as

$$W^{D1(3)}(Z_j, \bar{Z}_j) = W_0 \sum_{m=-\infty}^{+\infty} \left\{ I_m J_m(K_3 |\xi(Z_{1j})|) \left( \frac{\xi(Z_{1j})}{|\xi(Z_{1j})|} \right)^m \right\} \quad (41)$$

$$W^{D3(3)}(Z_j, \bar{Z}_j) = W_0 \sum_{m=-\infty}^{+\infty} \left\{ K_m H_m^1(K_3 |\xi(Z_{3j})|) \left( \frac{\xi(Z_{3j})}{|\xi(Z_{3j})|} \right)^m \right\} \quad (42)$$

$$W^{D4(3)}(Z_j, \bar{Z}_j) = W_0 \sum_{m=-\infty}^{+\infty} \left\{ M_m H_m^1(K_3 |\xi(Z_{4j})|) \left( \frac{\xi(Z_{4j})}{|\xi(Z_{4j})|} \right)^m \right\} \quad (43)$$

$$W^{D5(3)}(Z_j, \bar{Z}_j) = W_0 \sum_{m=-\infty}^{+\infty} \left\{ N_m H_m^1(K_3 |\xi(Z_{5j})|) \left( \frac{\xi(Z_{5j})}{|\xi(Z_{5j})|} \right)^m \right\} \quad (44)$$

Where

$$Z_{1j} = \begin{cases} Z_3 + b_{13} & j = 3 \\ Z_4 + b_{14} & j = 4 \\ Z_5 + b_{15} & j = 5 \end{cases} \quad Z_{3j} = \begin{cases} Z_1 + b_{31} & j = 1 \\ Z_4 + b_{34} & j = 4 \\ Z_5 + b_{35} & j = 5 \end{cases} \quad Z_{4j} = \begin{cases} Z_3 + b_{43} & j = 3 \\ Z_1 + b_{41} & j = 1 \\ Z_5 + b_{45} & j = 5 \end{cases} \quad Z_{5j} = \begin{cases} Z_3 + b_{53} & j = 3 \\ Z_1 + b_{51} & j = 1 \\ Z_4 + b_{54} & j = 4 \end{cases}$$

and  $b_{31} = H_1 + H_3 + (-L/2 + H_3 \tan(\alpha_4))i$ ,  $b_{34} = H_3 + (-L + H_3 \tan(\alpha_4))i$ ,  $b_{35} = H_3 + (H_3 \tan(\alpha_4))i$ ,  $b_{13} = -b_{31}$

$b_{14} = -H_1 - L/2i$ ,  $b_{15} = -H_1 + L/2i$ ,  $b_{43} = -b_{34}$ ,  $b_{41} = -b_{14}$ ,  $b_{45} = Li$ ,  $b_{53} = -b_{35}$ ,  $b_{51} = -b_{15}$ ,  $b_{54} = -b_{45}$

The corresponding shear stresses are:

$$\tau_{r_j z}^{D1(3)}(Z_j, \bar{Z}_j) = \sum_{m=-\infty}^{+\infty} \left\{ I_m \hat{P}_m^J(Z_{3j}) \right\}, \kappa = 0 \quad (45)$$

$$\tau_{\theta_j z}^{D1(3)}(Z_j, \bar{Z}_j) = \sum_{m=-\infty}^{+\infty} \left\{ I_m \hat{Q}_m^J(Z_{3j}) \right\}, \kappa = 0 \quad (46)$$

$$\tau_{r_j z}^{D3(3)}(Z_j, \bar{Z}_j) = \sum_{m=-\infty}^{+\infty} \left\{ K_m \hat{P}_m^{H1}(Z_{1j}) \right\}, \kappa = 0 \quad (47)$$

$$\tau_{\theta_j z}^{D3(3)}(Z_j, \bar{Z}_j) = \sum_{m=-\infty}^{+\infty} \left\{ K_m \hat{Q}_m^{H^1}(Z_{1j}) \right\}, \kappa = 0 \quad (48)$$

$$\tau_{r_j z}^{D4(3)}(Z_j, \bar{Z}_j) = \sum_{m=-\infty}^{+\infty} \left\{ M_m \hat{P}_m^{H^1}(Z_{4j}) \right\}, \kappa = 0 \quad (49)$$

$$\tau_{\theta_j z}^{D4(3)}(Z_j, \bar{Z}_j) = \sum_{m=-\infty}^{+\infty} \left\{ M_m \hat{Q}_m^{H^1}(Z_{4j}) \right\}, \kappa = 0 \quad (50)$$

$$\tau_{r_j z}^{D5(3)}(Z_j, \bar{Z}_j) = \sum_{m=-\infty}^{+\infty} \left\{ N_m \hat{P}_m^{H^1}(Z_{5j}) \right\}, \kappa = 0 \quad (51)$$

$$\tau_{\theta_j z}^{D5(3)}(Z_j, \bar{Z}_j) = \sum_{m=-\infty}^{+\infty} \left\{ N_m \hat{Q}_m^{H^1}(Z_{5j}) \right\}, \kappa = 0 \quad (52)$$

## 2.6 Wave function in region ④ and ⑤

There is only standing wave  $W^{D(\cdot)}$  in the closed region ④ or ⑤, it need satisfy governing Eq. (1) and free hypotenuse condition.

Reference formula Eq. (22), the ④ ⑤ region can be rewritten as

$$W^{D4(4)}(Z_j, \bar{Z}_j) = W_0 \sum_{m=0}^{+\infty} \left\{ F_m J_{mp_4}(K_4 |\xi(Z_{4j}) e^{q_4 i}|) \left[ \left( \frac{\xi(Z_{4j}) e^{q_4 i}}{|\xi(Z_{4j}) e^{q_4 i}|} \right)^{mp_4} + (-1)^m \left( \frac{\xi(Z_{4j}) e^{q_4 i}}{|\xi(Z_{4j}) e^{q_4 i}|} \right)^{-mp_4} \right] \right\} \quad (53)$$

$$W^{D5(5)}(Z_j, \bar{Z}_j) = W_0 \sum_{m=0}^{+\infty} \left\{ G_m J_{mp_5}(K_5 |\xi(Z_{5j}) e^{q_5 i}|) \left[ \left( \frac{\xi(Z_{5j}) e^{q_5 i}}{|\xi(Z_{5j}) e^{q_5 i}|} \right)^{mp_5} + (-1)^m \left( \frac{\xi(Z_{5j}) e^{q_5 i}}{|\xi(Z_{5j}) e^{q_5 i}|} \right)^{-mp_5} \right] \right\} \quad (54)$$

Where  $Z_{4j} = Z_4 + b_{44} \quad j = 4$  ,  $Z_{5j} = Z_5 + b_{55} \quad j = 5$  and  $q_4 = -(f(\alpha_6) + f(-\pi/2))/2$  ,  
 $q_5 = -(f(\pi/2) + f(\alpha_7))/2$  ,  $p_4 = \pi/(f(\alpha_6) - f(-\pi/2))$  ,  $p_5 = \pi/(f(\pi/2) - f(\alpha_7))$  ,  $b_{44} = b_{55} = 0$

The corresponding shear stresses are:

$$\tau_{r_j z}^{D4(4)}(Z_j, \bar{Z}_j) = \sum_{m=0}^{+\infty} \left\{ F_m \hat{P}_{mp_4}^J(Z_{4j}) \right\} \quad (55)$$

$$\tau_{\theta_j z}^{D4(4)}(Z_j, \bar{Z}_j) = \sum_{m=0}^{+\infty} \left\{ F_m \hat{Q}_{mp_4}^J(Z_{4j}) \right\} \quad (56)$$

$$\tau_{r_j z}^{D5(5)}(Z_j, \bar{Z}_j) = \sum_{m=0}^{+\infty} \left\{ G_m \hat{P}_{mp_5}^J(Z_{5j}) \right\} \quad (57)$$

$$\tau_{\theta_j z}^{D5(5)}(Z_j, \bar{Z}_j) = \sum_{m=0}^{+\infty} \left\{ G_m \hat{Q}_{mp_5}^J(Z_{5j}) \right\} \quad (58)$$

## 2.7 Wave function in region ⑥

According to Eq.(29), equation of scattered wave  $W^{D6(6)}$  generated by boundary  $D_6$  and satisfying governing Eq. (1) and free boundary condition  $C_3$  in the complex plane  $(z_j, \bar{z}_j)$  can be written as

$$W^{D6(6)}(Z_j, \bar{Z}_j) = W_0 \sum_{m=-\infty}^{+\infty} \left\{ A_m \left[ \begin{aligned} & \left[ J_m(K_6 |\zeta(Z_{9j}) - \zeta(H_4)|) \left( \frac{\zeta(Z_{9j}) - \zeta(H_4)}{|\zeta(Z_{9j}) - \zeta(H_4)|} \right)^m + \right. \\ & \left. (-1)^m J_m(K_6 |\zeta(Z_{9j}) + \bar{\zeta}(H_4)|) \left( \frac{\zeta(Z_{9j}) + \bar{\zeta}(H_4)}{|\zeta(Z_{9j}) + \bar{\zeta}(H_4)|} \right)^{-m} \right] \end{aligned} \right\} \quad (59)$$

Where  $Z_{9j} = Z_8 + b_{98}, j=8$  and  $b_{98} = H_4$ .

The corresponding shear stresses are:

$$\tau_{r_j z}^{D6(6)}(Z_j, \bar{Z}_j) = \sum_{m=0}^{+\infty} \left\{ A_m \hat{P}_m^J(Z_{9j}) \right\} \quad (60)$$

$$\tau_{\theta_j z}^{D6(6)}(Z_j, \bar{Z}_j) = \sum_{m=0}^{+\infty} \left\{ A_m \hat{Q}_m^J(Z_{9j}) \right\} \quad (61)$$

## 2.8 Boundary conditions and solving method

Based on the continuity conditions of displacement and stress at the auxiliary boundary  $D_1, D_3, D_4, D_5, D_6$ , and radial zero-stress at the hole edge  $D_2$ , a system of equations are established for solving the unknown complex coefficients.

$$\left\{ \begin{aligned} & W^{D6(1)}(Z_8, \bar{Z}_8) + W^{D3(1)}(Z_8, \bar{Z}_8) = W^{D6(6)}(Z_8, \bar{Z}_8) & Z_8 \in D_8 \\ & \tau_{r_3 z}^{D6(1)}(Z_8, \bar{Z}_8) + \tau_{r_3 z}^{D3(1)}(Z_8, \bar{Z}_8) = \tau_{r_3 z}^{D6(8)}(Z_8, \bar{Z}_8) & Z_8 \in D_8 \\ & W^{D6(1)}(Z_3, \bar{Z}_3) + W^{D3(1)}(Z_3, \bar{Z}_3) = W^{D1(3)}(Z_3, \bar{Z}_3) + W^{D3(3)}(Z_3, \bar{Z}_3) + W^{D4(3)}(Z_3, \bar{Z}_3) + W^{D5(3)}(Z_3, \bar{Z}_3) & Z_3 \in D_3 \\ & \tau_{r_3 z}^{D6(1)}(Z_3, \bar{Z}_3) + \tau_{r_3 z}^{D3(1)}(Z_3, \bar{Z}_3) = \tau_{r_3 z}^{D1(3)}(Z_3, \bar{Z}_3) + \tau_{r_3 z}^{D3(3)}(Z_3, \bar{Z}_3) + \tau_{r_3 z}^{D4(3)}(Z_3, \bar{Z}_3) + \tau_{r_3 z}^{D5(3)}(Z_3, \bar{Z}_3) & Z_3 \in D_3 \\ & W^{D4(4)}(Z_4, \bar{Z}_4) = W^{D1(3)}(Z_4, \bar{Z}_4) + W^{D3(3)}(Z_4, \bar{Z}_4) + W^{D4(3)}(Z_4, \bar{Z}_4) + W^{D5(3)}(Z_4, \bar{Z}_4) & Z_4 \in D_4 \\ & \tau_{r_4 z}^{D4(4)}(Z_4, \bar{Z}_4) = \tau_{r_4 z}^{D1(3)}(Z_4, \bar{Z}_4) + \tau_{r_4 z}^{D3(3)}(Z_4, \bar{Z}_4) + \tau_{r_4 z}^{D4(3)}(Z_4, \bar{Z}_4) + \tau_{r_4 z}^{D5(3)}(Z_4, \bar{Z}_4) & Z_4 \in D_4 \\ & W^{D5(5)}(Z_5, \bar{Z}_5) = W^{D1(3)}(Z_5, \bar{Z}_5) + W^{D3(3)}(Z_5, \bar{Z}_5) + W^{D4(3)}(Z_5, \bar{Z}_5) + W^{D5(3)}(Z_5, \bar{Z}_5) & Z_5 \in D_5 \\ & \tau_{r_5 z}^{D5(5)}(Z_5, \bar{Z}_5) = \tau_{r_5 z}^{D1(3)}(Z_5, \bar{Z}_5) + \tau_{r_5 z}^{D3(3)}(Z_5, \bar{Z}_5) + \tau_{r_5 z}^{D4(3)}(Z_5, \bar{Z}_5) + \tau_{r_5 z}^{D5(3)}(Z_5, \bar{Z}_5) & Z_5 \in D_5 \\ & W^{D1(2)}(Z_1, \bar{Z}_1) + W^{D2(2)}(Z_1, \bar{Z}_1) + W^{(i+r)}(Z_1, \bar{Z}_1) = W^{D1(3)}(Z_1, \bar{Z}_1) + W^{D3(3)}(Z_1, \bar{Z}_1) + W^{D4(3)}(Z_1, \bar{Z}_1) + W^{D5(3)}(Z_1, \bar{Z}_1) & Z_1 \in D_1 \\ & \tau_{r_1 z}^{D1(2)}(Z_1, \bar{Z}_1) + \tau_{r_1 z}^{D2(2)}(Z_1, \bar{Z}_1) + \tau_{r_1 z}^{(i+r)}(Z_1, \bar{Z}_1) = \tau_{r_1 z}^{D1(3)}(Z_1, \bar{Z}_1) + \tau_{r_1 z}^{D3(3)}(Z_1, \bar{Z}_1) + \tau_{r_1 z}^{D4(3)}(Z_1, \bar{Z}_1) + \tau_{r_1 z}^{D5(3)}(Z_1, \bar{Z}_1) & Z_1 \in D_1 \\ & \tau_{r_2 z}^{D1(2)}(Z_2, \bar{Z}_2) + \tau_{r_2 z}^{D2(2)}(Z_2, \bar{Z}_2) + \tau_{r_2 z}^{(i+r)}(Z_2, \bar{Z}_2) = 0 & Z_2 \in D_2 \end{aligned} \right. \quad (62)$$

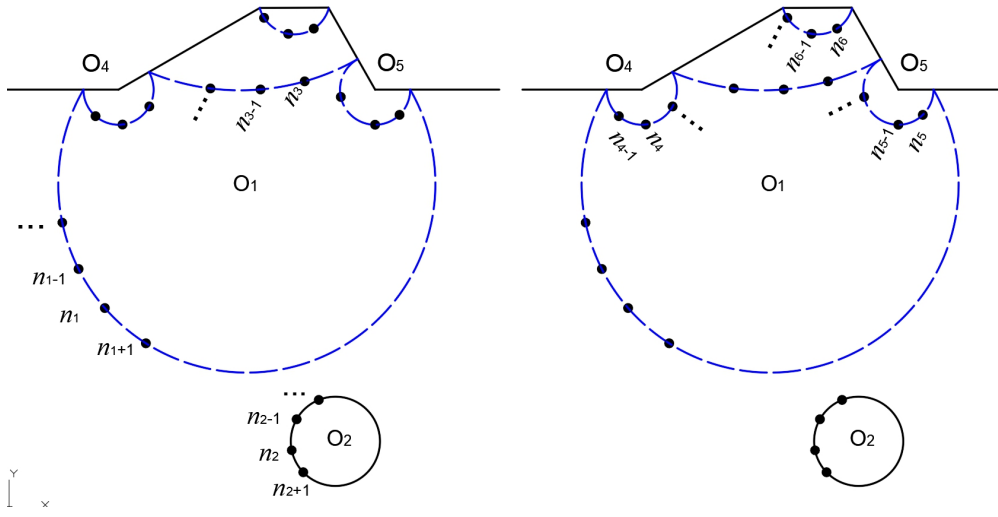


Fig 3. Discrete points of auxiliary boundary and hole edge

Currently, the fourier expansion method is commonly used to solve the undetermined coefficients of algebraic equations, and it is an average approximation of the entire boundary conditions. Due to the wave field high gradient of the trapezoid edge and multiple auxiliary boundaries, the fourier expansion method which convergence speed is slow is difficult to solve the problem of the scalene trapezoid. Therefore, this paper proposes least square method with direct discrete boundary conditions. Take discrete points according to the set distance on the boundary, and the displacement and stress on the two sides of the discrete points are equal, as shown in the figure. An infinite number of points  $n$  can be taken on the boundary to form an infinite number of equations to solve the undetermined coefficients  $A_m, B_m, C_m, \dots$ . In order to minimize the error of the undetermined coefficient of the finite term, a large number of sample points  $n$  ( $n \gg m$ ) are approximated to the true solution by the least square method. This paper uses equidistant discrete points and stress terms divided by  $\mu k$  (not reflected in the formula) to coordinate the weights of euclidean distance. The matrix is expressed as

$$\bar{M}^T M X = \bar{M}^T N \quad (63)$$

Where

$$M = \begin{bmatrix} a_{nm}^8 & -b_{nm}^8 & -c_{nm}^8 & 0 & 0 & 0 & 0 & 0 & 0 & 0 & 0 \\ a_{nm}^{8\tau} & -b_{nm}^{8\tau} & -c_{nm}^{8\tau} & 0 & 0 & 0 & 0 & 0 & 0 & 0 & 0 \\ 0 & -b_{nm}^3 & -c_{nm}^3 & 0 & 0 & 0 & 0 & i_{nm}^3 & k_{nm}^3 & m_{nm}^3 & n_{nm}^3 \\ 0 & -b_{nm}^{3\tau} & -c_{nm}^{3\tau} & 0 & 0 & 0 & 0 & i_{nm}^{3\tau} & k_{nm}^{3\tau} & m_{nm}^{3\tau} & n_{nm}^{3\tau} \\ 0 & 0 & 0 & 0 & 0 & -f_{nm}^4 & 0 & i_{nm}^4 & k_{nm}^4 & m_{nm}^4 & n_{nm}^4 \\ 0 & 0 & 0 & 0 & 0 & -f_{nm}^{4\tau} & 0 & i_{nm}^{4\tau} & k_{nm}^{4\tau} & m_{nm}^{4\tau} & n_{nm}^{4\tau} \\ 0 & 0 & 0 & 0 & 0 & 0 & g_{nm}^5 & i_{nm}^5 & k_{nm}^5 & m_{nm}^5 & n_{nm}^5 \\ 0 & 0 & 0 & 0 & 0 & 0 & g_{nm}^{5\tau} & i_{nm}^{5\tau} & k_{nm}^{5\tau} & m_{nm}^{5\tau} & n_{nm}^{5\tau} \\ 0 & 0 & 0 & -d_{nm}^1 & -e_{nm}^1 & 0 & 0 & i_{nm}^1 & k_{nm}^1 & m_{nm}^1 & n_{nm}^1 \\ 0 & 0 & 0 & -d_{nm}^{1\tau} & -e_{nm}^{1\tau} & 0 & 0 & i_{nm}^{1\tau} & k_{nm}^{1\tau} & m_{nm}^{1\tau} & n_{nm}^{1\tau} \\ 0 & 0 & 0 & -d_{nm}^{2\tau} & -e_{nm}^{2\tau} & 0 & 0 & 0 & 0 & 0 & 0 \end{bmatrix} \quad X = \begin{bmatrix} A_m \\ B_m \\ C_m \\ D_m \\ E_m \\ F_m \\ G_m \\ I_m \\ K_m \\ M_m \\ N_m \end{bmatrix} \quad N = \begin{bmatrix} 0 \\ 0 \\ 0 \\ 0 \\ 0 \\ 0 \\ 0 \\ 0 \\ 0 \\ \zeta_n^1 \\ \zeta_n^{1\tau} \\ \zeta_n^{2\tau} \end{bmatrix}$$

above formula see appendix for details.

## 2.9 Surface displacement amplitude and hole stress

In region ①, the total wave field  $W_1$  is

$$W_1 = W^{D3(1)} + W^{D6(1)} \quad (64)$$

In region ②, the total wave field  $W_2$  has three components:

$$W_2 = W^{D1(2)} + W^{D2(2)} + W^{(i+r)} \quad (65)$$

In region ③, the total wave field  $W_3$  has four components:

$$W_3 = W^{D1(3)} + W^{D3(3)} + W^{D4(3)} + W^{D5(3)} \quad (66)$$

In region ④, the total wave field  $W_4$  has four components:

$$W_4 = W^{D4(4)} \quad (67)$$

In region ⑤, the total wave field  $W_5$  has four components:

$$W_5 = W^{D5(5)} \quad (68)$$

In region ⑥, the total wave field  $W_6$  has four components:

$$W_6 = W^{D6(6)} \quad (69)$$

Eqs. (64) to (69) can also be expressed as

$$W_j = |W_j| e^{(\omega t - \phi_j)i} \quad j = 1, 2, \dots \quad (70)$$

Where  $|W_j|$  is the displacement amplitude,  $\phi_j$  is the phase angle of  $W_j$

$$\phi_j = \arctan(\text{Im}(W_j)/\text{Re}(W_j)) \quad (71)$$

The dimensionless frequency of incident waves can be expressed as

$$\eta = \frac{2L/2}{\lambda} = \frac{kL}{2\pi} \quad (72)$$

Where  $K_1=K_2=K_3=K_4=K_5=K_6=k$ , and  $k$  is given by Eqs. (11).  $\lambda$  is the wavelength of the incident waves. It is well known that the effect of elastic waves on surface displacement and hole stress highly relies on wavelength. As can be seen from Eq. (72), the dimensionless frequency  $\eta$  is introduced to represent the ratio of the radius ( $r_2$ ) of the hole to the wavelength, and indirectly represents the magnitude of the wave number.

In region ②, hole hoop stress can be expressed as

$$\tau_{\theta z} = \tau_{\theta z}^{D1(2)} + \tau_{\theta z}^{D2(2)} + \tau_{\theta z}^{(i+r)} \quad (73)$$

The dimensionless hoop stress is

$$\tau_{\theta z}^* = \left| \tau_{\theta z} / \tau_0 \right|, \quad |Z_2| = r_2 \quad (74)$$

Where  $\tau_0 = \mu k W_0$

### 3 Numerical examples and discussions

Table. 1 Parameters of scalene trapezoid and hole

Figure	$L$	$n_1$	$n_2$	$H$	$H_2$	$L_2$	$r_2$	$\kappa$	$\nu$
Fig 4~ Fig 6									
Fig 10, Fig 12	6.0	0.5	1.5	2.0	6.0	0.0	1.0	0.8	0.2
Fig 14~Fig 16									
Fig 19~Fig 21									
Fig 7	6.0	0.5	1.5	2.0	6.0	0.0	1.0	/	0.0
Fig 8	6.0	0.5	1.5	2.0	6.0	0.0	1.0	1.0	/
Fig 9	6.0	0.5	1.5	2.0	6.0	0.0	/	0.8	0.2
Fig 11, Fig 13	6.0	1.5	0.5	2.0	6.0	0.0	1.0	0.8	0.2
Fig 17	6.0	1.0	1.0	2.0	6.0	0.0	1.0	/	0.0
Fig 18	6.0	1.0	1.0	2.0	6.0	0.0	1.0	1.0	/

#### 3.1 Precision discussion

An important method to verify the theory is to fit the continuity of the auxiliary boundary and the zero-stress condition of the circular hole edge, free surface. The numerical results of auxiliary boundary, hole edge and free surface are given for frequency of incident  $\eta=2.0$ , incident angle  $\alpha=0^\circ$   $60^\circ$ (the max incident angle  $\alpha_{max} = \text{acot}(2C_{45}/C_{55}) = 68^\circ$ ), trapezoidal edge slope  $n_1=0.5$   $n_2=1.5$ ,

material parameters  $\kappa=0.8$   $\nu=0.2$  ( $\kappa=C_{44}/C_{55}$ ,  $\nu=C_{45}/C_{55}$ ). As shown in Fig 4 to Fig 5, the displacement  $W$  and stress  $\tau_{rz}^*$  continuity of the auxiliary boundary  $D$  are good, and the stress  $\tau_{\theta z}^*$  of the surface and  $\tau_{rz}^*$  of the circular hole boundary  $D_2$  are close to 0, which indicate that the wave function and the least square method are effective.

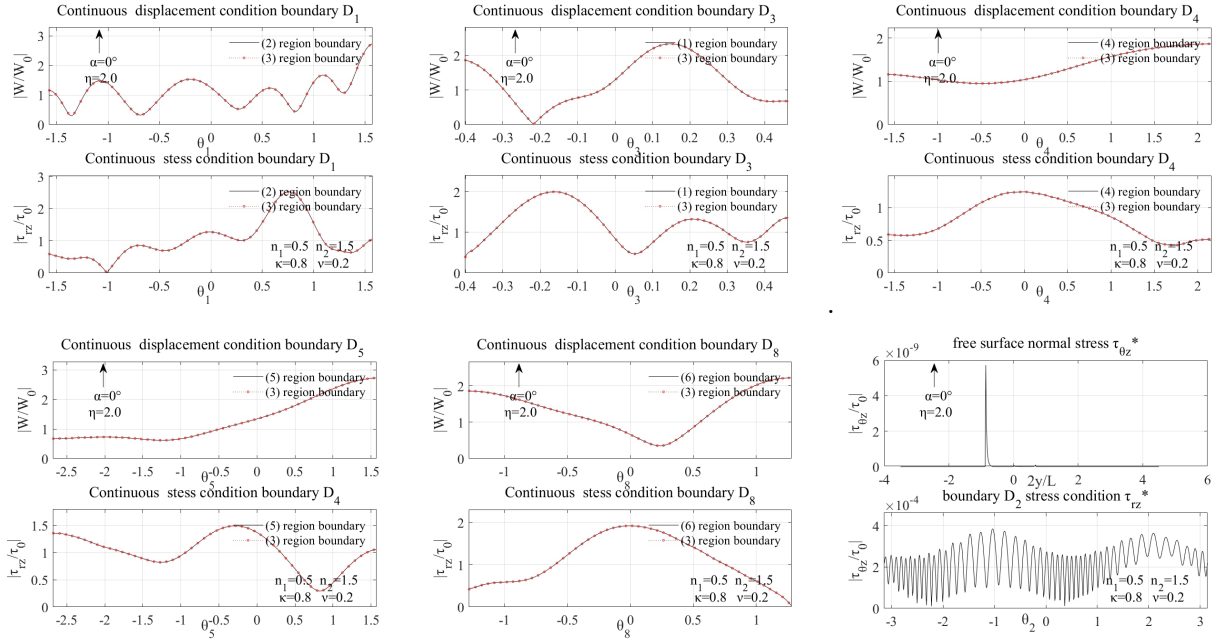


Fig 4. The continuity of the auxiliary boundary and free edge zero-stress at  $\alpha=0^\circ$

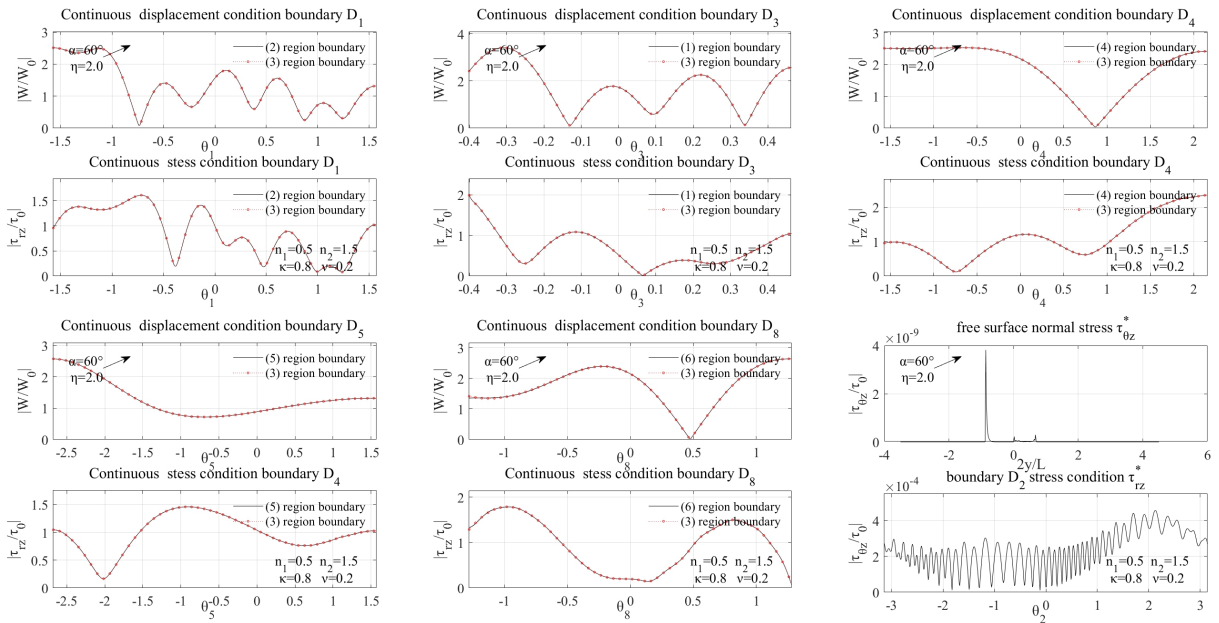


Fig 5. The continuity of the auxiliary boundary and free edge zero-stress at  $\alpha=60^\circ$

Another important method to verify the theory is to compare with the solution results of the finite element method as shown in Fig 6 which display the free surface displacement amplitudes  $|W/W_0|$ , hole edge stress  $\tau_{\theta z}^*$  and displacement cloud at a certain time. The FEM results are obtained

by the commercial software Ls-Dyna with user-defined material models. The geometric model is meshed by shell element which edge length 0.1 and grid only with out-of-plane translational degree of freedom. The mesh area is large enough to eliminate the effects of boundary reflections. Sine excitation is applied to the bottom or right edge of the analysis area, corresponding to incident angle  $0^\circ$  or  $-90^\circ$ , and the calculation time is long enough to ensure that it is in a steady state. The surface displacement magnitude measures from the displacement of the surface element nodes, and the stress of the finite element hole edge comes from the stress of the nearest element of the hole edge, which represents the stress in the hole edge area rather than the hole edge. So the FEM stress results may be a bit inaccurate. For incident angle  $\alpha=-90^\circ$ , it is difficult to obtain a sufficient reflected wave area near the surface due to limitation of computational grid domain and computer computing power. Therefore, the finite element analysis results are only for reference. The results by the proposed method are agree with those by the finite element method from figure.

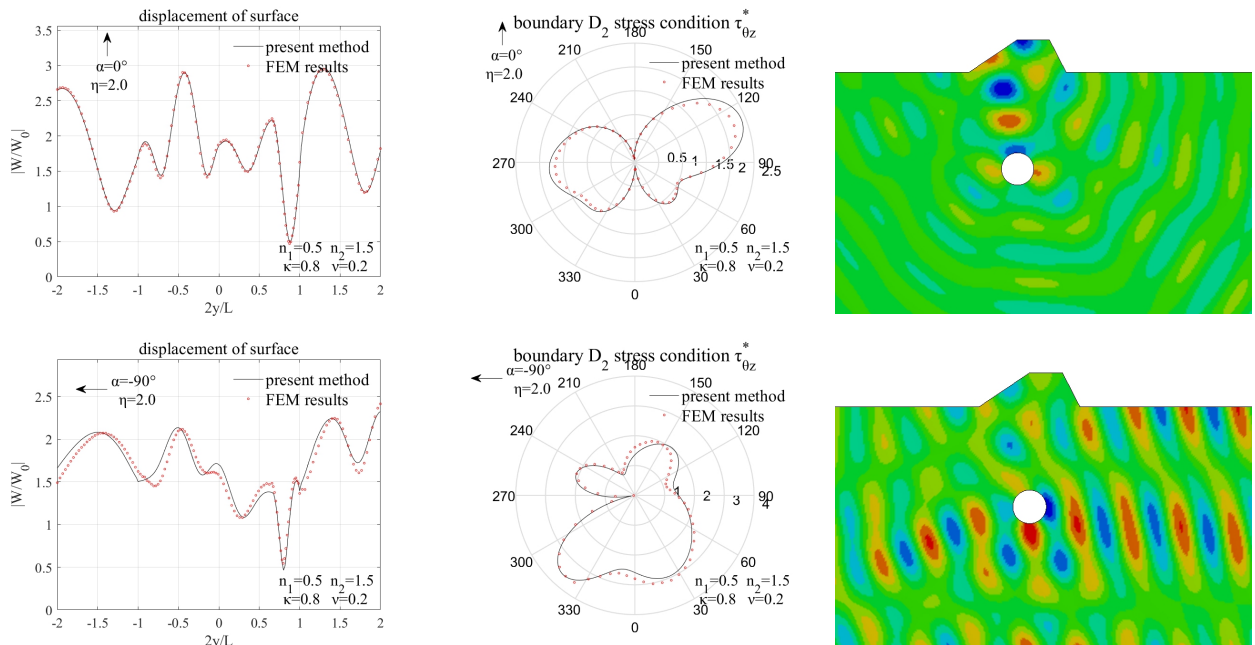


Fig 6. Comparisons of the proposed solution results with FEM results at  $\eta=0.5$   $n_1=0.5$

### 3.2 Numerical examples and analysis

Each position of free surface can be expressed by dimensionless  $y/(L/2)$  in the cartesian coordinate system  $o_6x_6y_6$ , where -1 represents the left trapezoid foot point,  $2n_2H/L-1$  is trapezoid left vertex,  $1-2n_1H/L$  is trapezoid right vertex, 1 represents the right trapezoid foot point.

#### (1) The characteristics of mapping function

It can be known from the anisotropic material coordinate system  $(x,y)$  and the isotropic material mapping coordinate system  $(x',y')$  that the shape of the trapezoid and the hole changes with

$\kappa$  or  $\nu$ . In the isotropic material space  $\kappa$  only changes the mapping coordinate  $x$  expansion ratio;  $\nu$  affects the scaling of the mapping coordinates  $x$  and  $y$ .

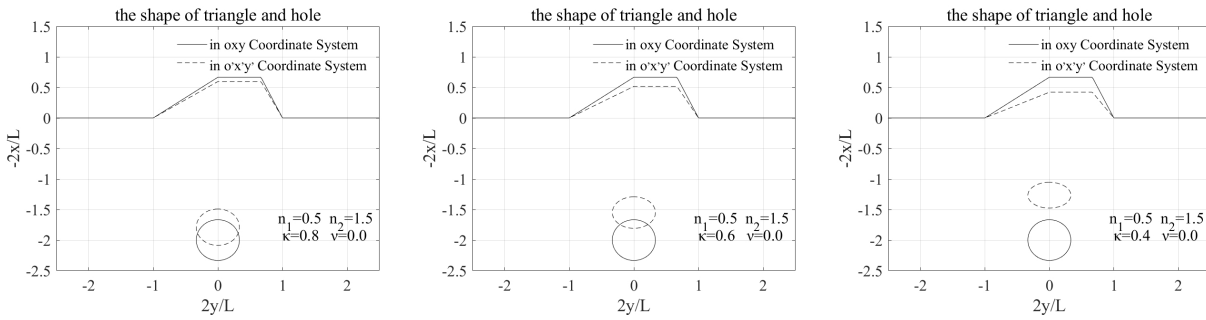


Fig 7. The shape of trapezoid and hole vs  $\kappa$

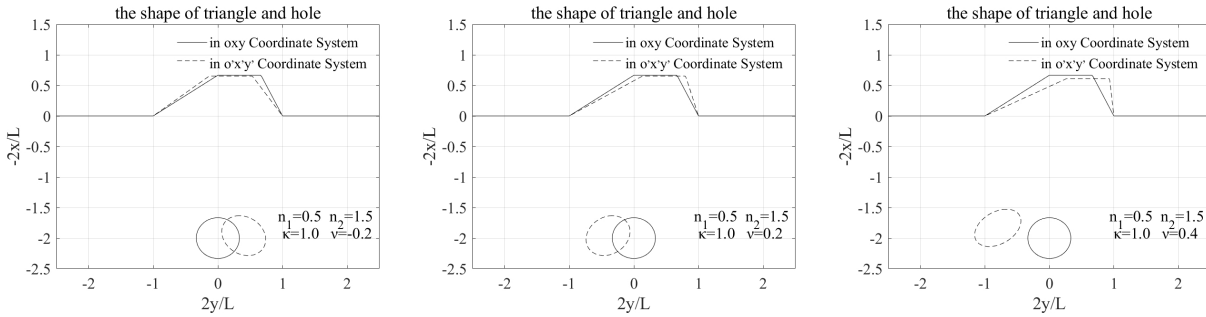


Fig 8. The shape of trapezoid and hole vs  $\nu$

## (2) The comparin of hole

It can be seen from the below figure that the hole has a small impact on the surface at low frequencies, while it has a greater impact at high frequencies, and the impact of the hole on the ground surface increases as the angle of incidence increases at low frequencies.

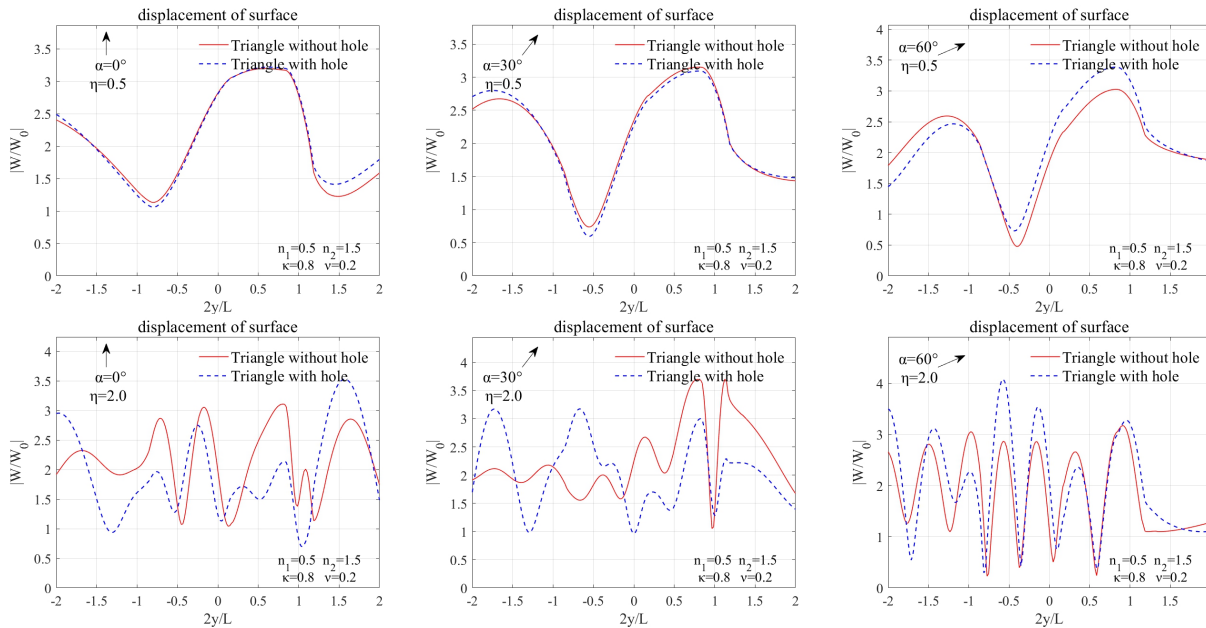


Fig 9. Free surface displacement amplitudes  $|W_j|$  of trapezoid without hole and with hole

## (3) The influence of materials

Free surface displacement amplitude and circular hole hoop stress distribution at different incident frequencies, angle and slope are shown in Fig 10 to Fig 13. When the incident wave has a horizontal component ( $\alpha \neq 0^\circ$ ), the amplitude and oscillation frequency of the right-side surface ( $2y/L > 1.0$ ) both decrease, while it increase in the incident wave side ( $2y/L < -1.0$ ). It seems that the trapezoid and the circle hole become filters and amplifier, and it is related to the angle of incidence and the slope of the trapezoid. This is due to the multiple reflections of the incident wave at different angles on different slopes. Both the amplitude and oscillation frequency of the trapezoidal area ( $-1.0 < 2y/L < 1.0$ ) are improved to different degrees.

The circular hole hoop stress distribution is quite different for different materials. So hole stress is very sensitive to material, while it is smaller at incident angle  $30^\circ$ .

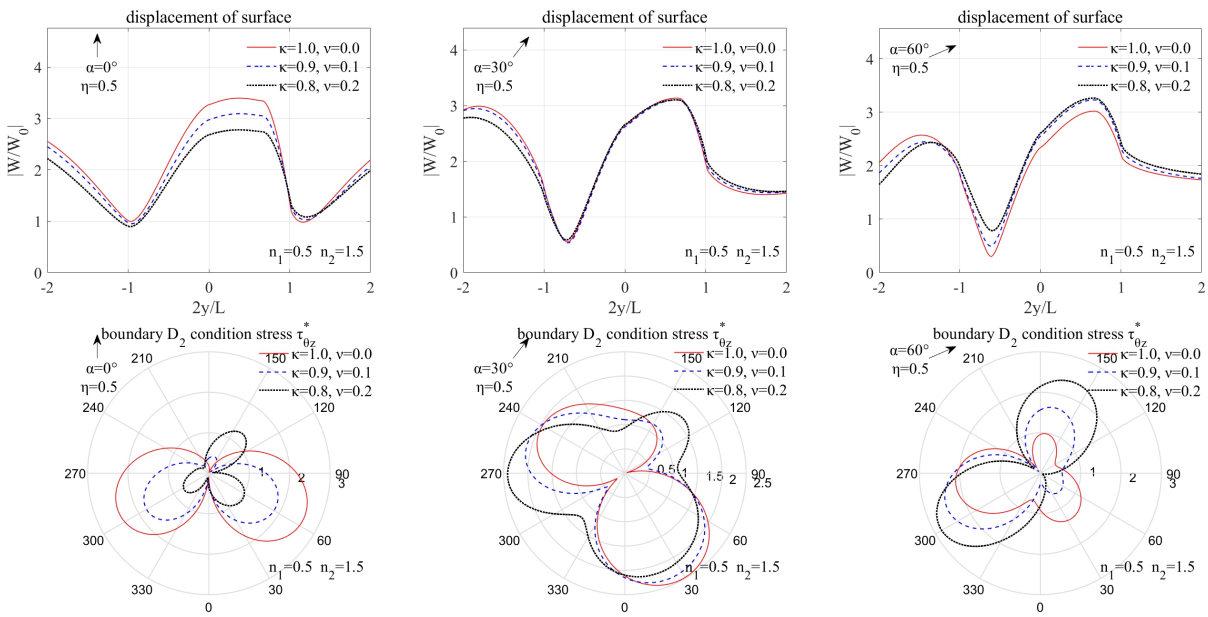


Fig 10. Free surface displacement amplitudes  $|W_j|$  and hole edge stress  $\tau_{\theta z}^*$  at  $\eta=0.5$   $n_1=0.5$

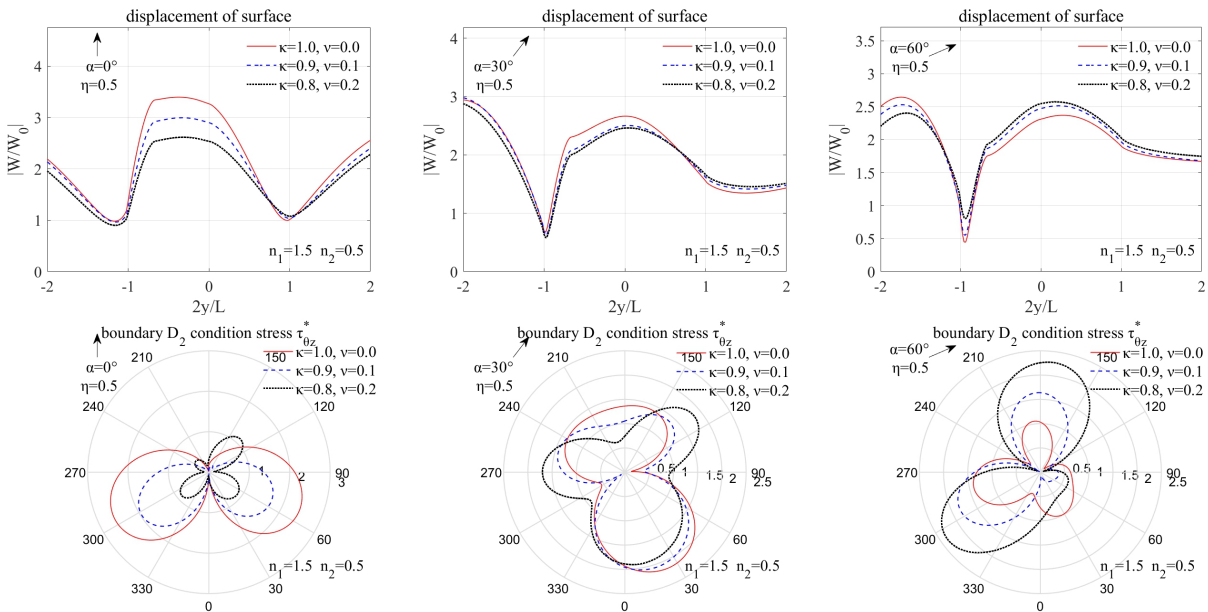


Fig 11. Free surface displacement amplitudes  $|W_j|$  and hole edge stress  $\tau_{\theta z}^*$  at  $\eta=0.5$   $n_1=1.5$

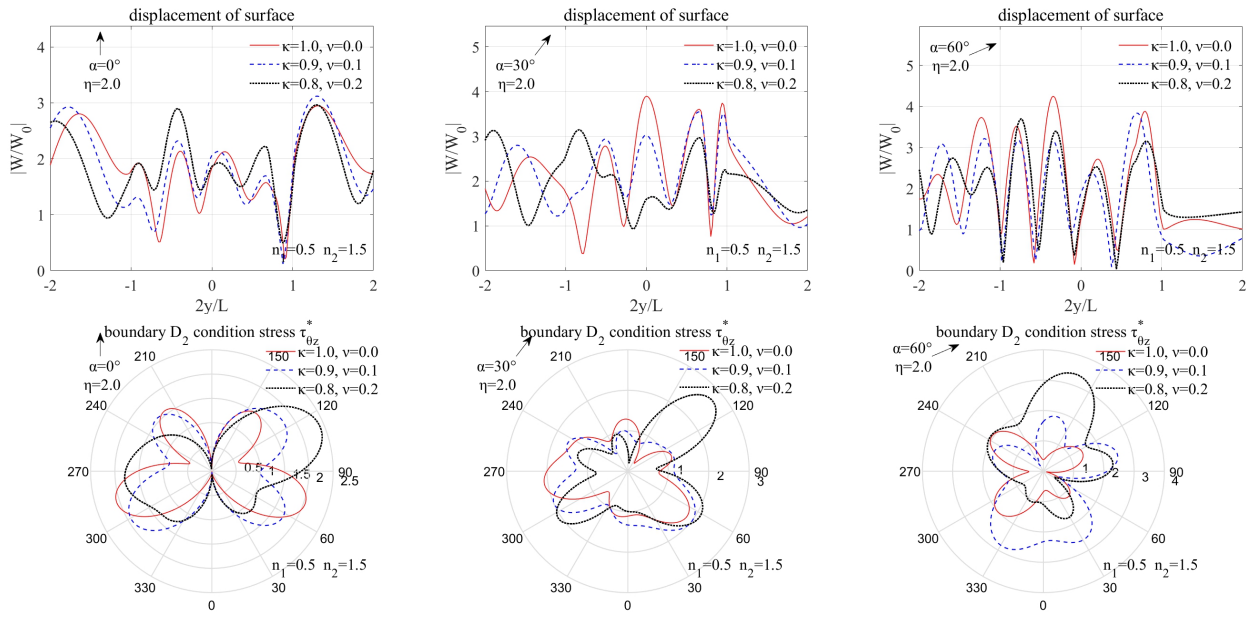


Fig 12. Free surface displacement amplitudes  $|W_j|$  and hole edge stress  $\tau_{\theta z}^*$  at  $\eta=2.0$   $n_1=0.5$

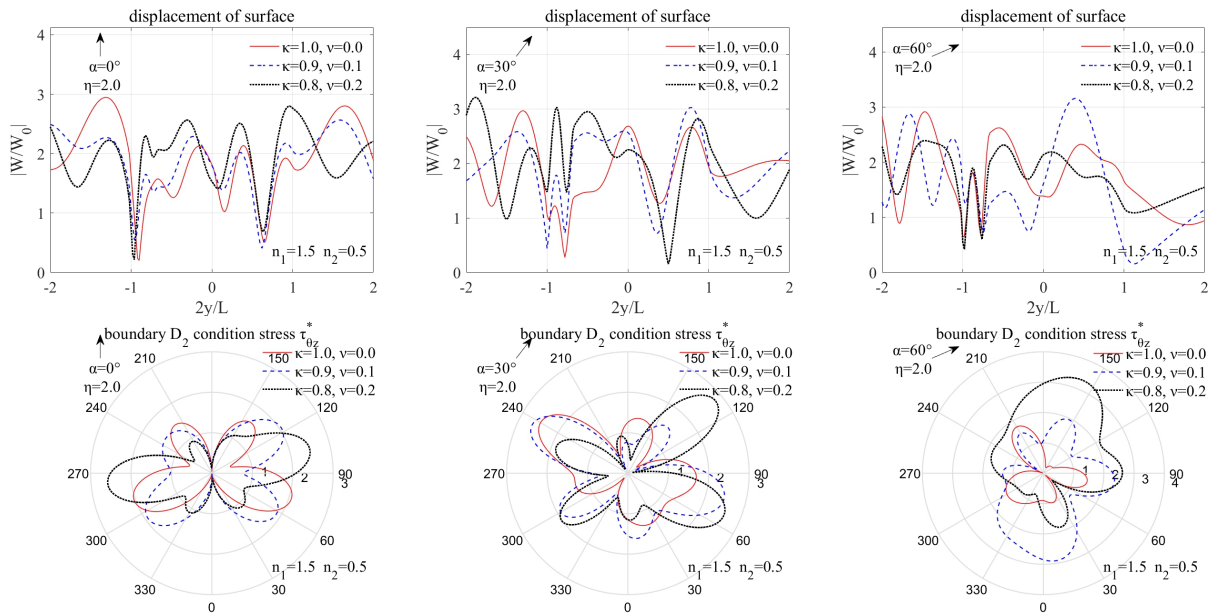


Fig 13. Free surface displacement amplitudes  $|W_j|$  and hole edge stress  $\tau_{\theta z}^*$  at  $\eta=2.0$   $n_1=1.5$

#### (4) The influence of hole deep

Free surface displacement amplitude and circular hole hoop stress distribution at different incident frequencies, angle and hole deep are shown in Fig 14 and Fig 15. When the incident angle  $\alpha=30^\circ$ , the amplitude of the surface displacement decreases as the hole depth increases, while the displacement amplitude of the triangular area increases. This is mainly due to the deeper the hole, the more wave energy enters trapezoid area. The change in hole stress is large at each incidence

angle. And it is still a big influence to free surface and hole stress even the hole deep reach to 20 from figure.

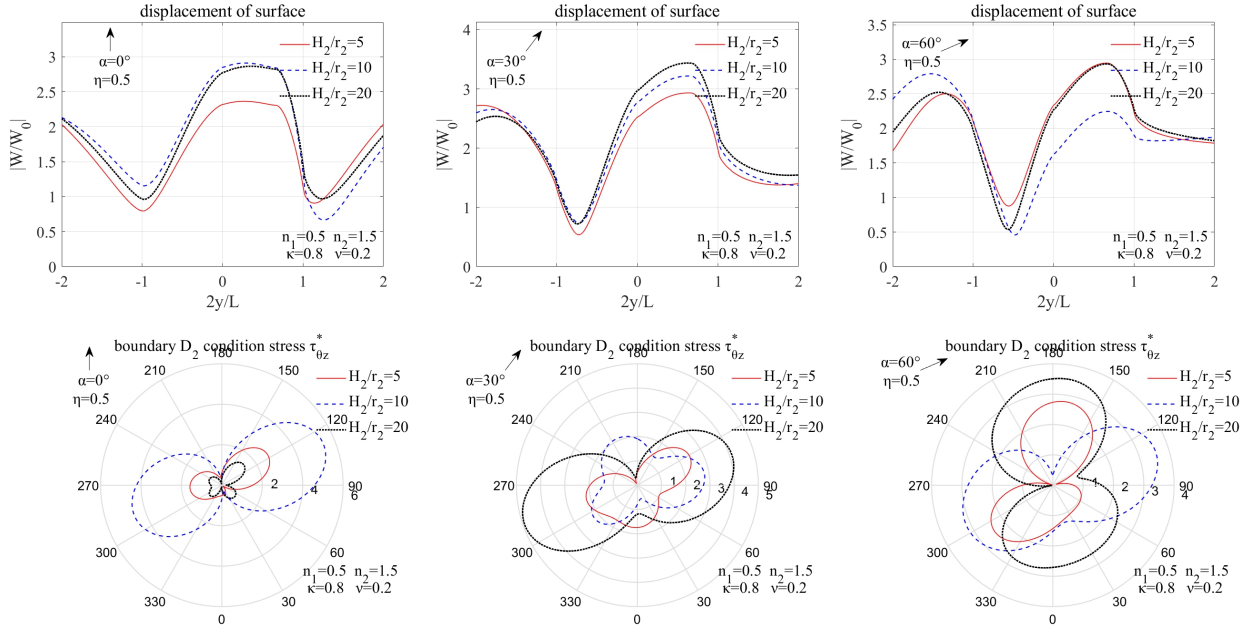


Fig 14. Free surface displacement amplitudes  $|W_j|$  and hole edge stress  $\tau_{\theta z}^*$  for various  $H_3$  at  $\eta=0.5$   $n_1=0.5$

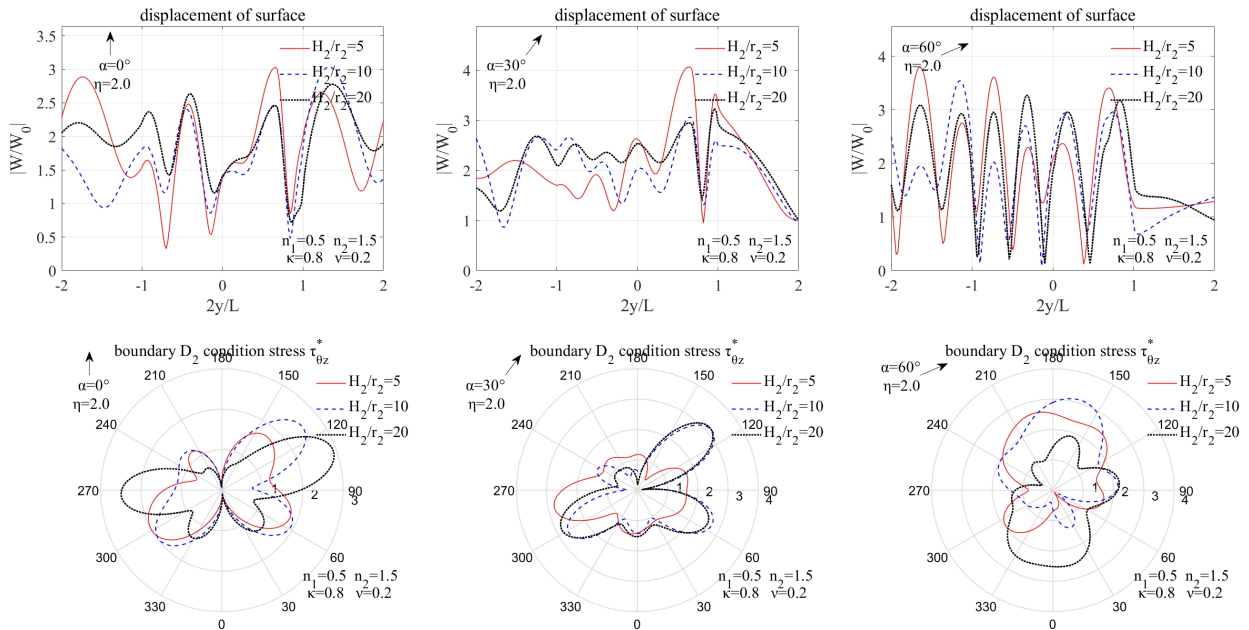


Fig 15. Free surface displacement amplitudes  $|W_j|$  and hole edge stress  $\tau_{\theta z}^*$  for various  $H_3$  at  $\eta=2.0$   $n_1=0.5$

(5) the influence of incident waves frequency

For the sake of revealing the influence of dimensionless frequencies on free surface displacement and hole stress, the first row pictures of Fig 16 give the displacement amplitudes as a function of  $2y/L$  and  $\eta$  at various angles of incidence ( $\alpha=0^\circ, 30^\circ, 60^\circ$ ) and slope ( $n_1=0.5$ ), and the second row pictures give the hole stress as a function of  $\theta$  and  $\eta$ . It shows that the number of wave peaks in the trapezoidal region increases as the wave dimensionless frequencies increases, and the peak and oscillation frequency increase on one side of the incident wave, while it decrease on the another side. At the same time, the peak and oscillation frequency of the area near the larger trapezoidal slope significantly increase, but when the angle of incidence changes large, the increase will move to the side of wave incoming direction. The hole concentrated stress is distributed on both sides of the wave propagation direction, and the shear stress near the free surface boundary is greater than that on the infinite space. This is because the superposition of the incident wave and the reflection wave of free boundary. The displacement amplitude of the trapezoidal surface is peak shape, and the displacement amplitude of the free flat surface is mountains shape which ridge is fluctuations.

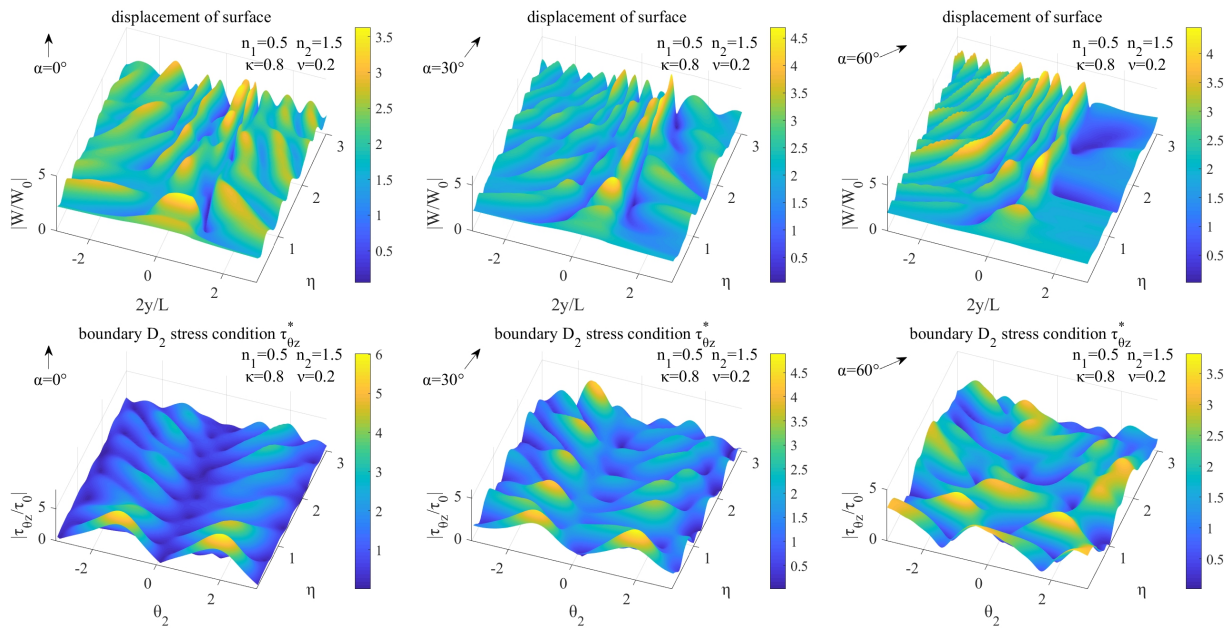


Fig 16. 3D plots of surface displacement amplitudes  $|W_j|$  and hole edge stress  $\tau_{\theta z}^*$  vs  $\eta$  at  $n_1=0.5$   
 $\kappa=0.8$

#### (6) the influence of $\kappa$

For the sake of revealing the influence of material parameters on free surface displacement and hole stress, the first row pictures of Fig 17 give the displacement amplitudes as a function of  $2y/L$  and  $\kappa$  at various angles of incidence ( $\alpha=0^\circ, 30^\circ, 60^\circ$ ) and slope ( $n_1=1.0$ ), and the second row pictures give the hole stress as a function of  $\theta$  and  $\kappa$ . It shows that the surface displacement and hole stress have an increasing trend as the  $\kappa$  decreases, but this trend gradually weakens as the incident

angle increases. The number of free surface displacement peaks decreases as  $k$  increases, while the number of hole stress peaks increases.

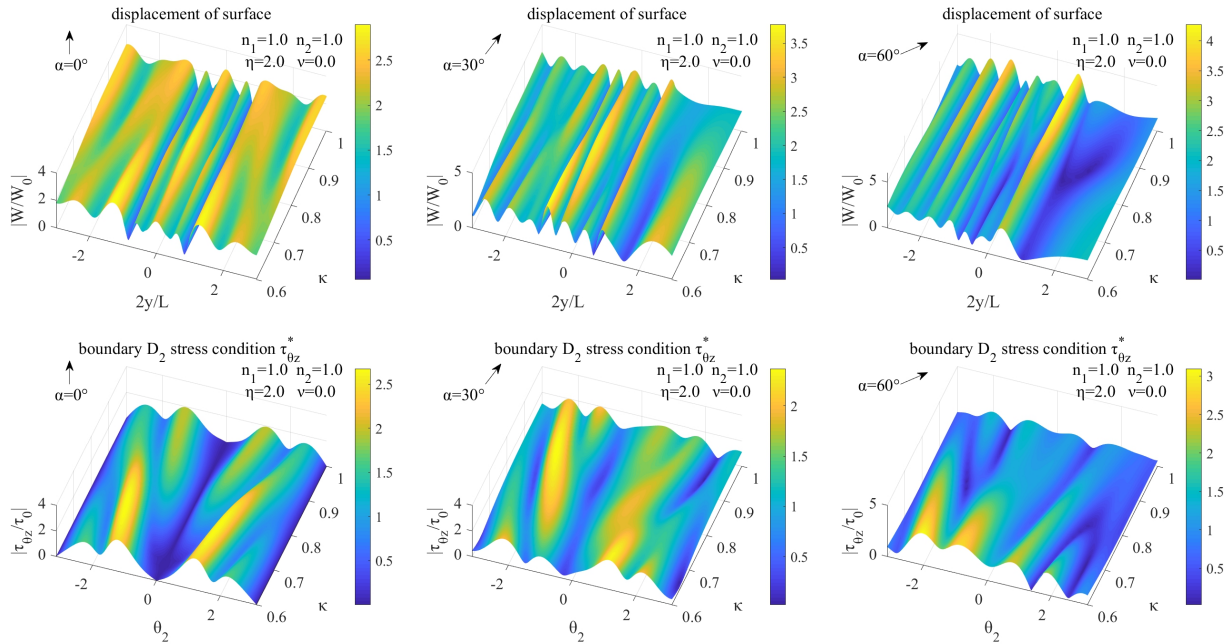
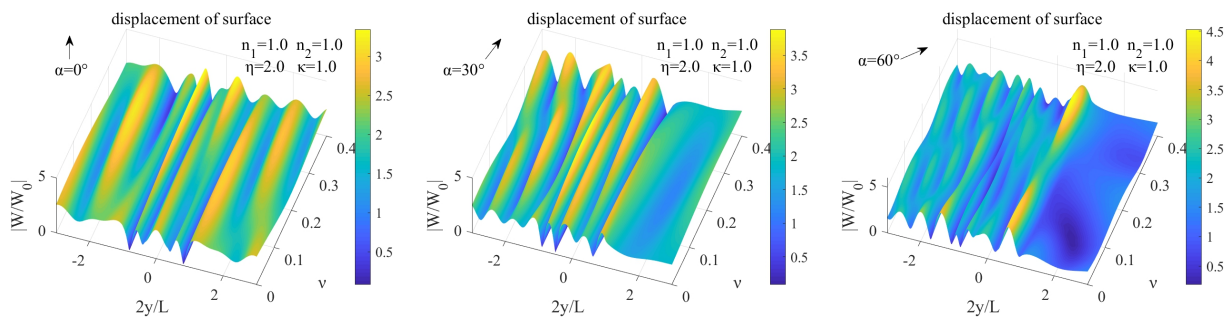


Fig 17. 3D plots of surface displacement amplitudes  $|W_j|$  and hole edge stress  $\tau_{\theta z}^*$  vs  $\kappa$  at  $\eta=2.0$   
 $n_1=1.0$   $v=0.0$

### (7) The influence of $v$

The first row pictures of Fig 18 give the displacement amplitudes as a function of  $2y/L$  and  $v$  at various angles of incidence ( $\alpha=0^\circ, 30^\circ, 60^\circ$ ) and slope ( $n_1=1.0$ ), and the second row pictures give the hole stress as a function of  $\theta$  and  $v$ . There is no obvious regular change in surface displacement and hole stress as  $v$  changes, and the overall level is at the same.



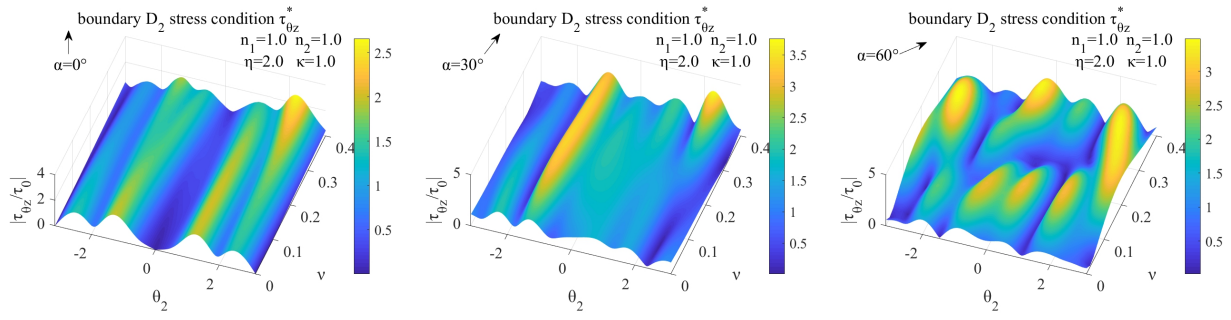


Fig 18. 3D plots of surface displacement amplitudes  $|W_j|$  and hole edge stress  $\tau_{\theta z}^*$  vs  $v$  at  $\eta=2.0$   
 $n_1=1.0$   $\kappa=1.0$

### 3.3 Time domain response

The transient response is obtained from the frequency domain results through the inverse fourier transform (IFT) algorithm. The incident time signal is a Ricker wavelet

$$Ri(t) = \left(1 - 2\pi^2 f_c^2 t^2\right) e^{-\pi^2 f_c^2 t^2} \quad (75)$$

with the characteristic frequency  $f_c=0.5\text{Hz}$ .

The calculated frequencies range from 0.0 to 2.0 Hz with 1/33 Hz intervals. The transfer function for every position is deduced in the previous chapter for a particular frequency  $\omega$  (or wave number  $k$ ). Then the time domain results can be synthesized by using the inverse FFT, and the shear wave propagates with the velocity  $c_T = 3$ . Fig 19 the reference point is set to be  $(x,y)=(8,-16)$  for  $t=0$  s, Fig 20 and Fig 21 the reference point are set to be  $(x,y)=(20,-15)$  for  $t=0$  s. The  $(x,y)$  reference coordinate system is  $o_6x_6y_6$ .

Fig 19 shows the synthetic displacement contour which half-space between  $y=-12$  to 12 and contains 800 discrete positions located along the surface of the trapezoid. Because the reference point is  $(8,-16)$ , the vertical Ricker wave reaches the flat surface ( $x=0$ ) at  $t=2.3\text{s}$  ( $c_{si} = 3.44$ ), after the vertical wave leave away from the flat surface several scattered waves appear one after another which amplitude of the scattered waves are obviously different. The incident angle  $60^\circ$  Ricker wave reaches the flat surface position ( $y=-12$ ) at  $t=2.6\text{s}$  ( $c_{si} = 2.83$ ), when the wave reach the trapezoid several scattered waves appear one after another which amplitude of the scattered waves are also obviously different.

In Fig 20 and Fig 21, compute snapshots for nodes with equally distance 0.05 at incident angle  $0^\circ$  and  $60^\circ$ . The snapshots show the wave fields at 9 specified times to illustrate the process of the wave propagation and scattering around a trapezoid shape and shallow circle. And the shape of circular hole scattered wave is non-circular, which is the biggest difference from a homogeneous medium. Besides, through the time domain results of various points, it can be used for the transient

response analysis of underground structures or surface structures to provide support for strength design.

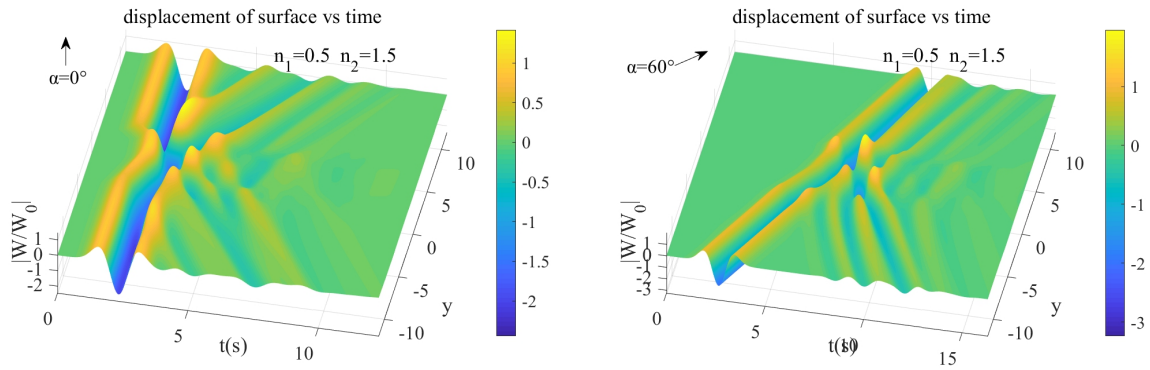


Fig 19. 3D plots of surface displacement amplitudes  $|W_j|$  vs time at  $n_1=0.5$

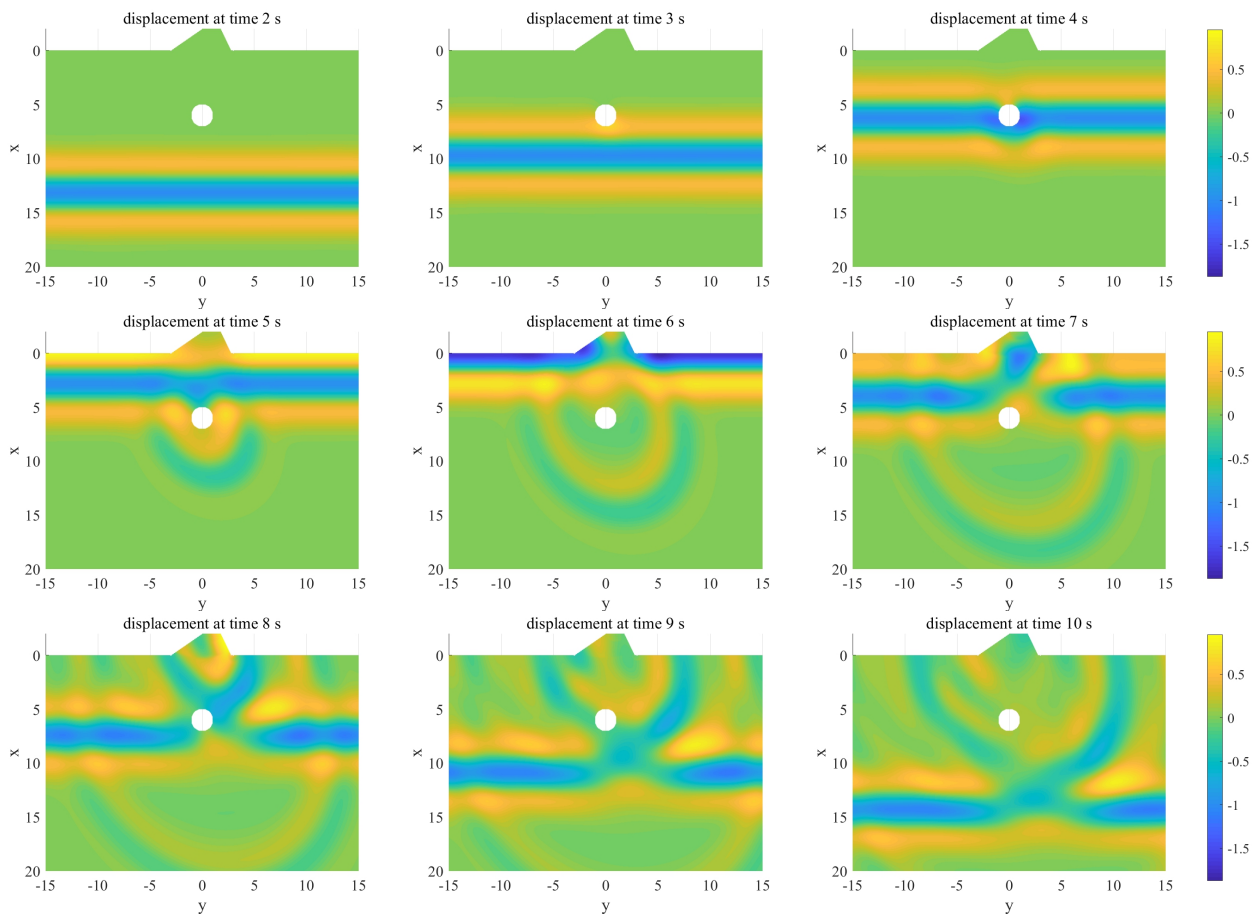


Fig 20. Snapshots for  $\alpha = 0^\circ$  at 9 specified times.

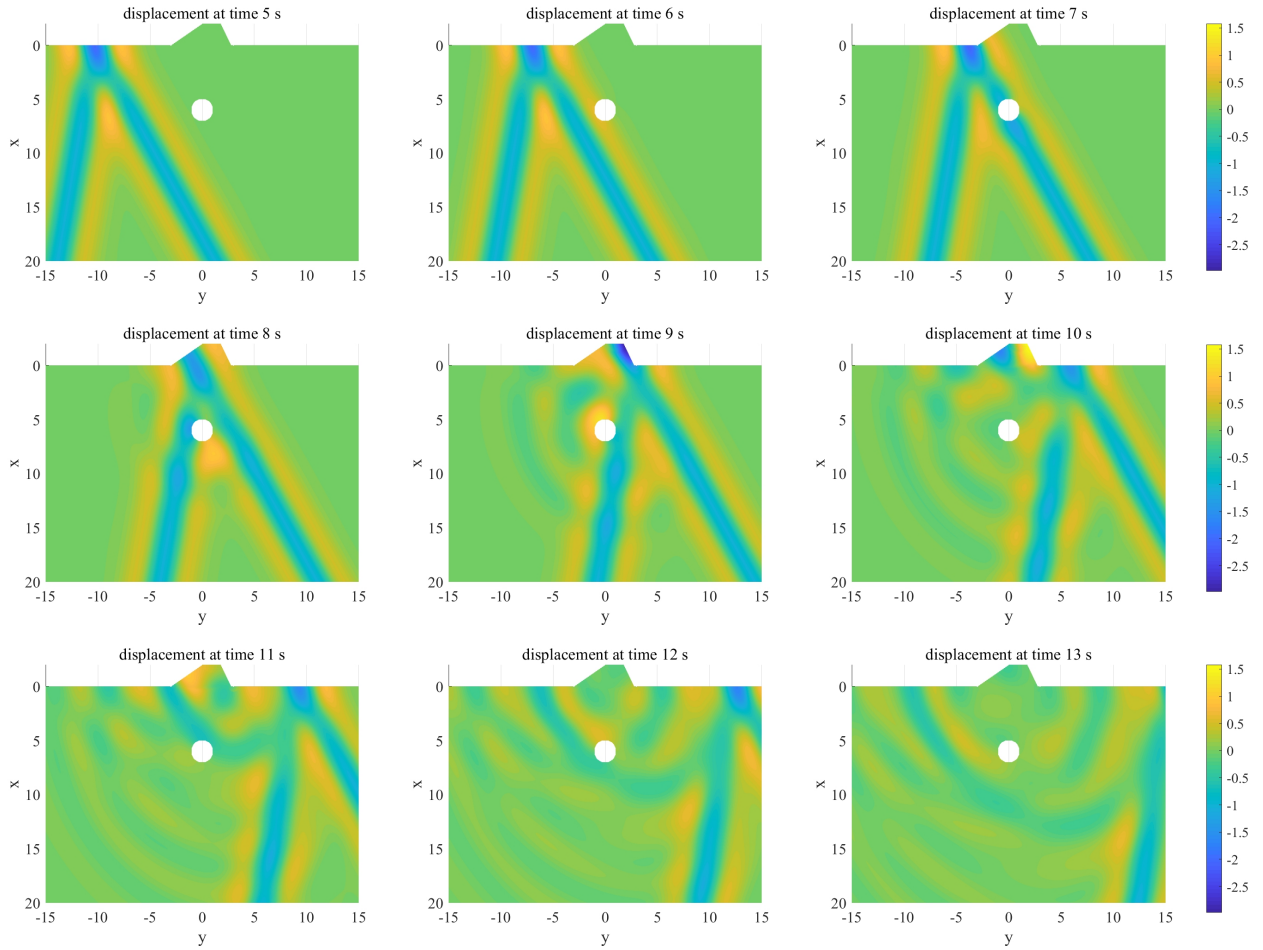


Fig 21. Snapshots for  $\alpha = 60^\circ$  at 9 specified times.

#### 4. Conclusions

This paper derives the mapping function, which transforms from anisotropic space to isotropic space. Using the mapping space and adopting the symmetric method, the zero-stress boundary condition of the semi-infinite cavity is solved. Finally, using complex variable function coordinate transformation, area matching method and least square method, the analytic solution of the wave to the typical scalene trapezoid boundary is obtained in frequency domain. From formula derivation and numerical simulation, the following conclusions can be drawn:

(1) It can be seen from the derivation that there are four mapping functions, that is, there are four mapping spaces, and each mapping function can solve the problem. Therefore, we can carry out further research on cracks and special-shaped cavities in the mapping space, just like dealing with a homogeneous medium.

(2) Because the anisotropic medium changes the direction of wave propagation, the incident angle  $\alpha_i$  can only be less than  $\text{acot}(2C_{45}/C_{55})$  near the free surface, and it can be used for shock absorption design.

(3) From the simulation effect, it can be found that  $\kappa$  determines the y-scaling of the geometric figure, and  $\nu$  determines the rotation of the image.

---

(4) When the incident angle  $\alpha=30^\circ$ , the amplitude of the surface displacement decreases as the hole depth increases, while the displacement amplitude of the trapezoidal area increases.

(5) The displacement amplitude of the trapezoidal surface is peak shape, while the displacement amplitude of the free flat surface is mountains shape which ridge is fluctuations. The number of wave peaks in the triangular region increases as the wave dimensionless frequencies increases, and the peak and oscillation frequency increase on one side of the incident wave, while it decrease on the another side. The hole concentrated stress is distributed on both sides of the wave propagation direction, and the shear stress near the free boundary is greater than that on the infinite space.

(6) The snapshots show the process of the wave propagation and scattering around trapezoid and shallow circle in time domain. Besides, through the time domain results of various points, it can be used for the transient response analysis of underground structures or surface structures to provide support for structural strength design.

## **5 Acknowledgments**

This work is supported by the National Key Research and Development Program of China (Grant No. 2019YFC1509301), the National Natural Science Foundation of China (Grant No. 11872156), the Fundamental Research Funds for the Central Universities and the program for Innovative Research Team in China Earthquake Administration.

## **6 Conflict of interest**

The authors declare that they have no known competing financial interests or personal relationships that could have appeared to influence the work reported in this paper.

## Appendix A: expressions of each angle in figure 1 model

$$\alpha_1 = \arctan(n_1), \quad \alpha_2 = \arctan(n_2), \quad \alpha_3 = \pi - \arctan\left(\frac{L+r_4+r_5}{2H_1}\right), \quad \alpha_4 = \alpha_1$$

$$\alpha_5 = \pi - 2\angle O_3 X_5 X_4 - \alpha_1, \quad \alpha_6 = \pi - \alpha_2, \quad \alpha_7 = \pi - \alpha_1, \quad \alpha_8 = -\arctan\left(\frac{L_T}{2H_4}\right)$$

Where

$$\angle O_3 X_5 X_4 = \arccos\left(\frac{L_{X_5 X_4}^2 + L_{X_5 O_3}^2 - L_{O_3 X_4}^2}{2L_{X_5 X_4} L_{X_5 O_3}}\right), \quad L_{X_5 X_4} = \sqrt{[r_5 \cos(\alpha_1) - r_4 \cos(\alpha_2)]^2 + [L - r_5 \sin(\alpha_1) - r_4 \sin(\alpha_2)]^2},$$

$$H = L/(n_1 + n_2), \quad L_T = (H - H_L)(n_1 + n_2), \quad L_{O_3 X_4} = H/\cos(\alpha_2) - r_4, \quad L_{O_3 X_5} = H/\cos(\alpha_1) - r_5,$$

$$r_3 = L_{X_5 X_4} / (2 * \sin((\alpha_4 + \alpha_5)/2)), \quad H_3 = (r_3 + \cos(\alpha_2)r_4 / \cos(\alpha_5)) \cos(\alpha_5)$$

## Appendix B: expressions of functions

$$a_{nm}^8 = W_0 \mathbf{J}_m \left( K_6 \left| \zeta(Z_8 + b_{98}) - \zeta(H_4) \right| \right) \left( \frac{\zeta(Z_8 + b_{98}) - \zeta(H_4)}{\left| \zeta(Z_8 + b_{98}) - \zeta(H_4) \right|} \right)^m + (-1)^m \mathbf{J}_m \left( K_6 \left| \zeta(Z_8 + b_{98}) + \zeta(H_4) \right| \right) \left( \frac{\zeta(Z_8 + b_{98}) + \zeta(H_4)}{\left| \zeta(Z_8 + b_{98}) + \zeta(H_4) \right|} \right)^{-m} \Bigg|_{\substack{|Z_8|=r_8 \\ -\alpha_8 \leq \varphi_n(Z_8) \leq \alpha_8}} \quad (\text{b1})$$

$$b_{nm}^8 = W_0 \mathbf{H}_{mp_0}^1 \left( K_1 \left| \zeta(Z_8 + b_{08}) e^{q_0 i} \right| \right) \left[ \left( \frac{\zeta(Z_8 + b_{08}) e^{q_0 i}}{\left| \zeta(Z_8 + b_{08}) e^{q_0 i} \right|} \right)^{mp_0} + (-1)^m \left( \frac{\zeta(Z_8 + b_{08}) e^{q_0 i}}{\left| \zeta(Z_8 + b_{08}) e^{q_0 i} \right|} \right)^{-mp_0} \right] \Bigg|_{\substack{|Z_8|=r_8 \\ -\alpha_8 \leq \varphi_n(Z_8) \leq \alpha_8}} \quad (\text{b2})$$

$$c_{nm}^8 = W_0 \mathbf{J}_{mp_0} \left( K_1 \left| \zeta(Z_8 + b_{08}) e^{q_0 i} \right| \right) \left[ \left( \frac{\zeta(Z_8 + b_{08}) e^{q_0 i}}{\left| \zeta(Z_8 + b_{08}) e^{q_0 i} \right|} \right)^{mp_0} + (-1)^m \left( \frac{\zeta(Z_8 + b_{08}) e^{q_0 i}}{\left| \zeta(Z_8 + b_{08}) e^{q_0 i} \right|} \right)^{-mp_0} \right] \Bigg|_{\substack{|Z_8|=r_8 \\ -\alpha_8 \leq \varphi_n(Z_8) \leq \alpha_8}} \quad (\text{b3})$$

$$a_{nm}^{8r} = \hat{P}_m^J(Z_8 + b_{98}) \Bigg|_{\substack{|Z_8|=r_8 \\ -\alpha_8 \leq \varphi_n(Z_8) \leq \alpha_8}} \quad (\text{b4})$$

$$b_{nm}^{8r} = \hat{P}_{mp_0}^{H_1}(Z_8 + b_{08}) \Bigg|_{\substack{|Z_8|=r_8 \\ -\alpha_8 \leq \varphi_n(Z_8) \leq \alpha_8}} \quad (\text{b5})$$

$$c_{nm}^{8r} = \hat{P}_{mp_0}^J(Z_8 + b_{08}) \Bigg|_{\substack{|Z_8|=r_8 \\ -\alpha_8 \leq \varphi_n(Z_8) \leq \alpha_8}} \quad (\text{b6})$$

$$b_{nm}^3 = W_0 \mathbf{H}_{mp_0}^1 \left( K_1 \left| \zeta(Z_3 + b_{03}) e^{q_0 i} \right| \right) \left[ \left( \frac{\zeta(Z_3 + b_{03}) e^{q_0 i}}{\left| \zeta(Z_3 + b_{03}) e^{q_0 i} \right|} \right)^{mp_0} + (-1)^m \left( \frac{\zeta(Z_3 + b_{03}) e^{q_0 i}}{\left| \zeta(Z_3 + b_{03}) e^{q_0 i} \right|} \right)^{-mp_0} \right] \Bigg|_{\substack{|Z_3|=r_3 \\ -\alpha_5 \leq \varphi_n(Z_3) \leq \alpha_4}} \quad (\text{b7})$$

$$c_{nm}^3 = W_0 \mathbf{J}_{mp_0} \left( K_1 \left| \zeta(Z_3 + b_{03}) e^{q_0 i} \right| \right) \left[ \left( \frac{\zeta(Z_3 + b_{03}) e^{q_0 i}}{\left| \zeta(Z_3 + b_{03}) e^{q_0 i} \right|} \right)^{mp_0} + (-1)^m \left( \frac{\zeta(Z_3 + b_{03}) e^{q_0 i}}{\left| \zeta(Z_3 + b_{03}) e^{q_0 i} \right|} \right)^{-mp_0} \right] \Bigg|_{\substack{|Z_3|=r_3 \\ -\alpha_5 \leq \varphi_n(Z_3) \leq \alpha_4}} \quad (\text{b8})$$

$$i_{nm}^3 = W_0 \mathbf{J}_m \left( K_3 \left| \zeta(Z_3 + b_{13}) \right| \right) \left( \frac{\zeta(Z_3 + b_{13})}{\left| \zeta(Z_3 + b_{13}) \right|} \right)^m \Bigg|_{\substack{|Z_3|=r_3 \\ -\alpha_5 \leq \varphi_n(Z_3) \leq \alpha_4}} \quad (\text{b9})$$

$$k_{nm}^3 = W_0 \mathbf{H}_m^1 \left( K_3 \left| \zeta(Z_3) \right| \right) \left( \frac{\zeta(Z_3)}{\left| \zeta(Z_3) \right|} \right)^m \Bigg|_{\substack{|Z_3|=r_3 \\ -\alpha_5 \leq \varphi_n(Z_3) \leq \alpha_4}} \quad (\text{b10})$$

$$m_{nm}^3 = W_0 \mathbf{H}_m^1 \left( K_3 \left| \zeta(Z_3 + b_{43}) \right| \right) \left( \frac{\zeta(Z_3 + b_{43})}{\left| \zeta(Z_3 + b_{43}) \right|} \right)^m \Bigg|_{\substack{|Z_3|=r_3 \\ -\alpha_5 \leq \varphi_n(Z_3) \leq \alpha_4}} \quad (\text{b11})$$

$$n_{nm}^3 = W_0 \mathbf{H}_m^1 \left( K_3 \left| \zeta(Z_3 + b_{53}) \right| \right) \left( \frac{\zeta(Z_3 + b_{53})}{\left| \zeta(Z_3 + b_{53}) \right|} \right)^m \Bigg|_{\substack{|Z_3|=r_3 \\ -\alpha_5 \leq \varphi_n(Z_3) \leq \alpha_4}} \quad (\text{b12})$$

$$b_{nm}^{3\tau} = \hat{\mathbf{P}}_{mp_0}^{H_1} \left( \zeta(Z_3 + b_{03}) \right) \Bigg|_{\substack{|Z_3|=r_3 \\ -\alpha_5 \leq \varphi_n(Z_3) \leq \alpha_4}} \quad (\text{b13})$$

$$c_{nm}^{3\tau} = \hat{\mathbf{P}}_{mp_0}^J \left( \zeta(Z_3 + b_{03}) \right) \Bigg|_{\substack{|Z_3|=r_3 \\ -\alpha_5 \leq \varphi_n(Z_3) \leq \alpha_4}} \quad (\text{b14})$$

$$i_{nm}^{3\tau} = \hat{\mathbf{P}}_m^J \left( \zeta(Z_3 + b_{13}) \right) \Bigg|_{\substack{|Z_3|=r_3 \\ -\alpha_5 \leq \varphi_n(Z_3) \leq \alpha_4}}, \lambda=0 \quad (\text{b15})$$

$$k_{nm}^{3\tau} = \hat{\mathbf{P}}_m^{H_1} \left( \zeta(Z_3) \right) \Bigg|_{\substack{|Z_3|=r_3 \\ -\alpha_5 \leq \varphi_n(Z_3) \leq \alpha_4}}, \lambda=0 \quad (\text{b16})$$

$$m_{nm}^{3\tau} = \hat{\mathbf{P}}_m^{H_1} \left( \zeta(Z_3 + b_{43}) \right) \Bigg|_{\substack{|Z_3|=r_3 \\ -\alpha_5 \leq \varphi_n(Z_3) \leq \alpha_4}}, \lambda=0 \quad (\text{b17})$$

$$n_{nm}^{3\tau} = \hat{\mathbf{P}}_m^{H_1} \left( \zeta(Z_3 + b_{53}) \right) \Bigg|_{\substack{|Z_3|=r_3 \\ -\alpha_5 \leq \varphi_n(Z_3) \leq \alpha_4}}, \lambda=0 \quad (\text{b18})$$

$$f_{nm}^4 = W_0 \mathbf{J}_{mp_4} \left( K_4 \left| \zeta(Z_4) e^{q_4 i} \right| \right) \left[ \left( \frac{\zeta(Z_4) e^{q_4 i}}{\left| \zeta(Z_4) e^{q_4 i} \right|} \right)^{mp_4} + (-1)^m \left( \frac{\zeta(Z_4) e^{q_4 i}}{\left| \zeta(Z_4) e^{q_4 i} \right|} \right)^{-mp_4} \right] \Bigg|_{\substack{|Z_4|=r_4 \\ -\pi/2 \leq \varphi_n(Z_4) \leq \alpha_6}} \quad (\text{b19})$$

$$i_{nm}^4 = W_0 \mathbf{J}_m \left( K_3 \left| \zeta(Z_4 + b_{14}) \right| \right) \left( \frac{\zeta(Z_4 + b_{14})}{\left| \zeta(Z_4 + b_{14}) \right|} \right)^m \Bigg|_{\substack{|Z_4|=r_4 \\ -\pi/2 \leq \varphi_n(Z_4) \leq \alpha_6}} \quad (\text{b20})$$

$$k_{nm}^4 = W_0 \mathbf{H}_m^1 \left( K_3 \left| \zeta(Z_4 + b_{34}) \right| \right) \left( \frac{\zeta(Z_4 + b_{34})}{\left| \zeta(Z_4 + b_{34}) \right|} \right)^m \Bigg|_{\substack{|Z_4|=r_4 \\ -\pi/2 \leq \varphi_n(Z_4) \leq \alpha_6}} \quad (\text{b21})$$

$$m_{nm}^4 = W_0 \mathbf{H}_m^1 \left( K_3 \left| \zeta(Z_4) \right| \right) \left( \frac{\zeta(Z_4)}{\left| \zeta(Z_4) \right|} \right)^m \Bigg|_{\substack{|Z_4|=r_4 \\ -\pi/2 \leq \varphi_n(Z_4) \leq \alpha_6}} \quad (\text{b22})$$

$$n_{nm}^4 = W_0 \mathbf{H}_m^1 \left( K_3 \left| \zeta(Z_4 + b_{54}) \right| \right) \left( \frac{\zeta(Z_4 + b_{54})}{\left| \zeta(Z_4 + b_{54}) \right|} \right)^m \Bigg|_{\substack{|Z_4|=r_4 \\ -\pi/2 \leq \varphi_n(Z_4) \leq \alpha_6}} \quad (\text{b23})$$

$$f_{nm}^{4\tau} = \hat{P}_{mp_0}^J \left( \zeta(Z_4 + b_{04}) \right) \Big|_{\substack{|Z_4|=r_4 \\ -\pi/2 \leq \varphi_n(Z_4) \leq \alpha_6}} \quad (\text{b24})$$

$$i_{nm}^{4\tau} = \hat{P}_m^J \left( \zeta(Z_4 + b_{14}) \right) \Big|_{\substack{|Z_4|=r_4 \\ -\pi/2 \leq \varphi_n(Z_4) \leq \alpha_6}, \lambda=0} \quad (\text{b25})$$

$$k_{nm}^{4\tau} = \hat{P}_m^{H_1} \left( \zeta(Z_4 + b_{34}) \right) \Big|_{\substack{|Z_4|=r_4 \\ -\pi/2 \leq \varphi_n(Z_4) \leq \alpha_6}, \lambda=0} \quad (\text{b26})$$

$$m_{nm}^{4\tau} = \hat{P}_m^{H_1} \left( \zeta(Z_4) \right) \Big|_{\substack{|Z_4|=r_4 \\ -\pi/2 \leq \varphi_n(Z_4) \leq \alpha_6}, \lambda=0} \quad (\text{b27})$$

$$n_{nm}^{4\tau} = \hat{P}_m^{H_1} \left( \zeta(Z_4 + b_{54}) \right) \Big|_{\substack{|Z_4|=r_4 \\ -\pi/2 \leq \varphi_n(Z_4) \leq \alpha_6}, \lambda=0} \quad (\text{b28})$$

$$g_{nm}^5 = W_0 \mathbf{J}_{mp_5} \left( K_5 \left| \zeta(Z_5) e^{q_5 i} \right| \right) \left[ \left( \frac{\zeta(Z_5) e^{q_5 i}}{\left| \zeta(Z_5) e^{q_5 i} \right|} \right)^{mp_5} + (-1)^m \left( \frac{\zeta(Z_5) e^{q_5 i}}{\left| \zeta(Z_5) e^{q_5 i} \right|} \right)^{-mp_5} \right] \Big|_{\substack{|Z_5|=r_5 \\ -\alpha_7 \leq \varphi_n(Z_5) \leq \pi/2}} \quad (\text{b29})$$

$$i_{nm}^5 = W_0 \mathbf{J}_m \left( K_3 \left| \zeta(Z_5 + b_{15}) \right| \right) \left( \frac{\zeta(Z_5 + b_{15})}{\left| \zeta(Z_5 + b_{15}) \right|} \right)^m \Big|_{\substack{|Z_5|=r_5 \\ -\alpha_7 \leq \varphi_n(Z_5) \leq \pi/2}} \quad (\text{b30})$$

$$k_{nm}^5 = W_0 \mathbf{H}_m^1 \left( K_3 \left| \zeta(Z_5 + b_{35}) \right| \right) \left( \frac{\zeta(Z_5 + b_{35})}{\left| \zeta(Z_5 + b_{35}) \right|} \right)^m \Big|_{\substack{|Z_5|=r_5 \\ -\alpha_7 \leq \varphi_n(Z_5) \leq \pi/2}} \quad (\text{b31})$$

$$m_{nm}^5 = W_0 \mathbf{H}_m^1 \left( K_3 \left| \zeta(Z_5 + b_{45}) \right| \right) \left( \frac{\zeta(Z_5 + b_{45})}{\left| \zeta(Z_5 + b_{45}) \right|} \right)^m \Big|_{\substack{|Z_5|=r_5 \\ -\alpha_7 \leq \varphi_n(Z_5) \leq \pi/2}} \quad (\text{b32})$$

$$n_{nm}^5 = W_0 \mathbf{H}_m^1 \left( K_3 \left| \zeta(Z_5) \right| \right) \left( \frac{\zeta(Z_5)}{\left| \zeta(Z_5) \right|} \right)^m \Big|_{\substack{|Z_5|=r_5 \\ -\alpha_7 \leq \varphi_n(Z_5) \leq \pi/2}} \quad (\text{b33})$$

$$g_{nm}^{5\tau} = \hat{P}_{mp_0}^J \left( \zeta(Z_5 + b_{05}) \right) \Big|_{\substack{|Z_5|=r_5 \\ -\alpha_7 \leq \varphi_n(Z_5) \leq \pi/2}} \quad (\text{b34})$$

$$i_{nm}^{5\tau} = \hat{P}_m^J \left( \zeta(Z_5 + b_{15}) \right) \Big|_{\substack{|Z_5|=r_5 \\ -\alpha_7 \leq \varphi_n(Z_5) \leq \pi/2}, \lambda=0} \quad (\text{b35})$$

$$k_{nm}^{5\tau} = \hat{P}_m^{H_1} \left( \zeta(Z_5 + b_{35}) \right) \Big|_{\substack{|Z_5|=r_5 \\ -\alpha_7 \leq \varphi_n(Z_5) \leq \pi/2}, \lambda=0} \quad (\text{b36})$$

$$m_{nm}^{5\tau} = P_m^{H_1} \left( \zeta(Z_5 + b_{45}) \right) \Big|_{\substack{|Z_5|=r_5 \\ -\alpha_7 \leq \varphi_n(Z_5) \leq \pi/2}, \lambda=0} \quad (\text{b37})$$

$$n_{nm}^{5\tau} = \frac{\mu_5 K_3 W_0}{2} P_m^{H_1} \left( \zeta(Z_5) \right) \Big|_{\substack{|Z_5|=r_5 \\ -\alpha_7 \leq \varphi_n(Z_5) \leq \pi/2}, \lambda=0} \quad (\text{b38})$$

$$\begin{aligned}
d_{nm}^1 = W_0 & \left. \begin{aligned} & \mathbf{H}_m^1 (K_2 |\zeta(Z_1 + b_{61}) - \zeta(H_1)|) \left( \frac{\zeta(Z_1 + b_{61}) - \zeta(H_1)}{|\zeta(Z_1 + b_{61}) - \zeta(H_1)|} \right)^m \\ & + (-1)^m \mathbf{H}_m^1 (K_2 |\zeta(Z_1 + b_{61}) + \zeta(H_1)|) \left( \frac{\zeta(Z_1 + b_{61}) + \zeta(H_1)}{|\zeta(Z_1 + b_{61}) + \zeta(H_1)|} \right)^{-m} \end{aligned} \right|_{\substack{|Z_1|=\eta_1 \\ -\alpha_3 \leq \varphi_n(Z_1) \leq \alpha_3}} \\
\text{(b39) } e_{nm}^1 = W_0 & \left. \begin{aligned} & \mathbf{H}_m^1 (K_2 |\zeta(Z_1 + b_{71}) - \zeta(H_2)|) \left( \frac{\zeta(Z_1 + b_{71}) - \zeta(H_2)}{|\zeta(Z_1 + b_{71}) - \zeta(H_2)|} \right)^m \\ & + (-1)^m \mathbf{H}_m^1 (K_2 |\zeta(Z_1 + b_{71}) + \zeta(H_2)|) \left( \frac{\zeta(Z_1 + b_{71}) + \zeta(H_2)}{|\zeta(Z_1 + b_{71}) + \zeta(H_2)|} \right)^{-m} \end{aligned} \right|_{\substack{|Z_1|=\eta_1 \\ -\alpha_3 \leq \varphi_n(Z_1) \leq \alpha_3}} \quad (b40)
\end{aligned}$$

$$i_{nm}^1 = W_0 \mathbf{J}_m (K_3 |\zeta(Z_1)|) \left( \frac{\zeta(Z_1)}{|\zeta(Z_1)|} \right)^m \Big|_{\substack{|Z_1|=\eta_1 \\ -\alpha_3 \leq \varphi_n(Z_1) \leq \alpha_3}} \quad (b41)$$

$$k_{nm}^1 = W_0 \mathbf{H}_m^1 (K_3 |\zeta(Z_1 + b_{31})|) \left( \frac{\zeta(Z_1 + b_{31})}{|\zeta(Z_1 + b_{31})|} \right)^m \Big|_{\substack{|Z_1|=\eta_1 \\ -\alpha_3 \leq \varphi_n(Z_1) \leq \alpha_3}} \quad (b42)$$

$$m_{nm}^1 = W_0 \mathbf{H}_m^1 (K_3 |\zeta(Z_1 + b_{41})|) \left( \frac{\zeta(Z_1 + b_{41})}{|\zeta(Z_1 + b_{41})|} \right)^m \Big|_{\substack{|Z_1|=\eta_1 \\ -\alpha_3 \leq \varphi_n(Z_1) \leq \alpha_3}} \quad (b43)$$

$$n_{nm}^1 = W_0 \mathbf{H}_m^1 (K_3 |\zeta(Z_1 + b_{51})|) \left( \frac{\zeta(Z_1 + b_{51})}{|\zeta(Z_1 + b_{51})|} \right)^m \Big|_{\substack{|Z_1|=\eta_1 \\ -\alpha_3 \leq \varphi_n(Z_1) \leq \alpha_3}} \quad (b44)$$

$$d_{nm}^{1\tau} = \hat{\mathbf{P}}_{mp_0}^{H_1} (\zeta(Z_1 + b_{61})) \Big|_{\substack{|Z_1|=\eta_1 \\ -\alpha_3 \leq \varphi_n(Z_1) \leq \alpha_3}} \quad (b45)$$

$$e_{nm}^{1\tau} = \hat{\mathbf{P}}_{mp_0}^{H_1} (\zeta(Z_1 + b_{71})) \Big|_{\substack{|Z_1|=\eta_1 \\ -\alpha_3 \leq \varphi_n(Z_1) \leq \alpha_3}} \quad (b46)$$

$$i_{nm}^{1\tau} = \hat{\mathbf{P}}_m^J (Z_1) \Big|_{\substack{|Z_1|=\eta_1 \\ -\alpha_3 \leq \varphi_n(Z_1) \leq \alpha_3}}, \lambda=0 \quad (b47)$$

$$k_{nm}^{1\tau} = \hat{\mathbf{P}}_m^{H^1} (Z_1 + b_{31}) \Big|_{\substack{|Z_1|=\eta_1 \\ -\alpha_3 \leq \varphi_n(Z_1) \leq \alpha_3}}, \lambda=0 \quad (b48)$$

$$m_{nm}^{1\tau} = \hat{\mathbf{P}}_m^{H^1} (Z_1 + b_{41}) \Big|_{\substack{|Z_1|=\eta_1 \\ -\alpha_3 \leq \varphi_n(Z_1) \leq \alpha_3}}, \lambda=0 \quad (b49)$$

$$n_{nm}^{1\tau} = \hat{\mathbf{P}}_m^{H^1} (Z_1 + b_{51}) \Big|_{\substack{|Z_1|=\eta_1 \\ -\alpha_3 \leq \varphi_n(Z_1) \leq \alpha_3}}, \lambda=0 \quad (b50)$$

$$\zeta_{nm}^1 = W_0 e^{\frac{-iK_2^1}{2} ((Z_1 + b_{31}) e^{\alpha i} + \overline{(Z_1 + b_{31})} e^{-\alpha i})} + W_0 e^{\frac{iK_2^1}{2} ((Z_1 + b_{31}) e^{-\alpha i} + \overline{(Z_1 + b_{31})} e^{\alpha i})} \Big|_{\substack{|Z_1|=\eta_1 \\ -\alpha_3 \leq \varphi_n(Z_1) \leq \alpha_3}} \quad (b51)$$

$$\zeta_{nm}^{1\tau} = \frac{1}{2} \left\{ \left[ (C_{55} + C_{44}) U(Z_1 + b_{31}) + (C_{55} - C_{44} - 2C_{45}i) V(Z_1 + b_{31}) \right] e^{\theta i} + \left[ (C_{55} - C_{44} + 2C_{45}i) U(Z_1 + b_{31}) + (C_{55} + C_{44}) V(Z_1 + b_{31}) \right] e^{-\theta i} \right\} \Big|_{\substack{|Z_1|=\eta_1 \\ -\alpha_3 \leq \varphi_n(Z_1) \leq \alpha_3}} \quad (b52)$$

$$d_{nm}^{2\tau} = \hat{\mathbf{P}}_m^{H^1} (\zeta(Z_2 + b_{62})) \Big|_{\substack{|Z_2|=\eta_2 \\ -\pi \leq \varphi_n(Z_2) \leq \pi}} \quad (b53)$$

$$f_{nm}^{2r} = \hat{P}_m^{\mathbf{H}^i} \left( \zeta(Z_2 + b_{72}) \right) \Big|_{\substack{|Z_2|=r_2 \\ -\pi \leq \varphi_n(Z_2) \leq \pi}} \quad (\text{b54})$$

$$\zeta_n^{2r} = \frac{1}{2} \left\{ \left[ (C_{55} + C_{44})U(Z_2 + b_{32}) + (C_{55} - C_{44} - 2C_{45}i)V(Z_2 + b_{32}) \right] e^{\theta_2 i} + \left[ (C_{55} - C_{44} + 2C_{45}i)U(Z_2 + b_{32}) + (C_{55} + C_{44})V(Z_2 + b_{32}) \right] e^{-\theta_2 i} \right\} \Big|_{\substack{|Z_2|=r_2 \\ -\pi \leq \varphi_n(Z_2) \leq \pi}} \quad (\text{b55})$$

where  $|Z_j|$ ,  $\varphi_n(Z_j)$  represents the modulus and phase angle of complex numbers, respectively.

$$\begin{aligned} f_1^r &= \frac{1}{4} [(C_{55} + C_{44})(\bar{\gamma}_1) + (C_{55} - C_{44} - 2C_{45}i)(-\gamma_2)] & f_1^\theta &= \frac{1}{4} [(C_{55}i + C_{44}i)(\bar{\gamma}_1) + (C_{55}i - C_{44}i + 2C_{45})(-\gamma_2)] \\ f_2^r &= \frac{1}{4} [(C_{55} + C_{44})(-\bar{\gamma}_2) + (C_{55} - C_{44} - 2C_{45}i)(\gamma_1)] & f_2^\theta &= \frac{1}{4} [(C_{55}i + C_{44}i)(-\bar{\gamma}_2) + (C_{55}i - C_{44}i + 2C_{45})(\gamma_1)] \\ f_3^r &= \frac{1}{4} [(C_{55} - C_{44} + 2C_{45}i)(\bar{\gamma}_1) + (C_{55} + C_{44})(-\gamma_2)] & f_3^\theta &= \frac{1}{4} [(-C_{55}i + C_{44}i + 2C_{45})(\bar{\gamma}_1) + (-C_{55}i - C_{44}i)(-\gamma_2)] \\ f_4^r &= \frac{1}{4} [(C_{55} - C_{44} + 2C_{45}i)(-\bar{\gamma}_2) + (C_{55} + C_{44})(\gamma_1)] & f_4^\theta &= \frac{1}{4} [(-C_{55}i + C_{44}i + 2C_{45})(-\bar{\gamma}_2) + (-C_{55}i - C_{44}i)(\gamma_1)] \end{aligned} \quad (\text{b56})$$

$$P_t^{\mathbf{H}}(s) = \frac{W_0 k}{2} \left\{ \mathbf{H}_{t-1}(k|s'|) \left[ \frac{s'}{|s'|} \right]^{t-1} - (-1)^m \kappa \mathbf{H}_{t+1}(k|s) \left[ \frac{s}{|s|} \right]^{t-1} \right\} e^{qi} \quad (\text{b57})$$

$$Q_t^{\mathbf{H}}(s) = \frac{W_0 k}{2} \left\{ -\mathbf{H}_{t+1}(k|s') \left[ \frac{s'}{|s'|} \right]^{t+1} + (-1)^m \kappa \mathbf{H}_{t-1}(k|s) \left[ \frac{s}{|s|} \right]^{t+1} \right\} e^{-qi}$$

$$\hat{P}_t^{\mathbf{H}}(s) = (f_1^r P_t^{\mathbf{H}}(s) + f_2^r Q_t^{\mathbf{H}}(s)) e^{\theta_1 i} + (f_3^r P_t^{\mathbf{H}}(s) + f_4^r Q_t^{\mathbf{H}}(s)) e^{-\theta_1 i} \quad (\text{b58})$$

$$\hat{Q}_t^{\mathbf{H}}(s) = (f_1^\theta P_t^{\mathbf{H}}(s) + f_2^\theta Q_t^{\mathbf{H}}(s)) e^{\theta_1 i} + (f_3^\theta P_t^{\mathbf{H}}(s) + f_4^\theta Q_t^{\mathbf{H}}(s)) e^{-\theta_1 i}$$

Where  $s' = [\zeta(s) - \zeta(H_j)] e^{qi}$ ,  $s = [\zeta(s) + \bar{\zeta}(H_j)] e^{qi}$ ,  $H_j$  is the depth of the corresponding circle center from the surface, and take a negative value if it above the horizontal plane.  $\mathbf{H}$  is Bessel functions or Hankel function.

$$P_t^{\mathbf{H}}(s), Q_t^{\mathbf{H}}(s) \text{ represent } \frac{\partial w}{\partial \xi}, \frac{\partial w}{\partial \bar{\xi}}. \quad \kappa = \begin{cases} 0 & \text{given} \\ 1 & \text{else} \end{cases}$$

$$\begin{aligned} U(z_{3j}) &= \left( \frac{-iK_2^i}{2} e^{\alpha_i} \right) W_0 e^{\frac{-iK_2^i}{2}(z_{3j} e^{\alpha_i} + \bar{z}_{3j} e^{-\alpha_i})} + \left( \frac{iK_2^r}{2} e^{-\alpha_i} \right) W_0 e^{\frac{iK_2^r}{2}(z_{3j} e^{-\alpha_i} + \bar{z}_{3j} e^{\alpha_i})} \\ V(z_{3j}) &= \left( \frac{-iK_2^i}{2} e^{-\alpha_i} \right) W_0 e^{\frac{-iK_2^i}{2}(z_{3j} e^{\alpha_i} + \bar{z}_{3j} e^{-\alpha_i})} + \left( \frac{iK_2^r}{2} e^{\alpha_i} \right) W_0 e^{\frac{iK_2^r}{2}(z_{3j} e^{-\alpha_i} + \bar{z}_{3j} e^{\alpha_i})} \end{aligned} \quad (\text{b59})$$

Where  $U(z_{3j}), V(z_{3j})$  represent  $\frac{\partial w}{\partial z}, \frac{\partial w}{\partial \bar{z}}$

---

## References

1. Pao Y.H., Maw C.C.. Diffraction of Elastic Wave and Dynamic Stress Concentration, Crane and Russak. 1973; New York, 113-121
2. Trifunac M.D.. Scattering of plane SH waves by a semi-cylindrical canyon. *Earthq. Eng. Struct. Dyn.* 1973; 1: 267–281.
3. Liu D.K., Han F. Scattering of plane SH-wave by cylindrical canyon of arbitrary shape. *Soil Dynamics and Earthquake Engineering.* 1991; 10: 5.
4. Yuan X., Liao Z.. Scattering of plane SH waves by a cylindrical canyon of circular-arc cross-section. *Soil Dyn. Earthq. Eng.* 1994;13: 407–412.
5. Lee V.W., Wu X.Y.. Application of the weighted residual method to diffraction by 2-D canyons of arbitrary shape:I. Incident SH waves. *Soil Dynamics and Earthquake Engineering.* 1994; 13:355-364.
6. Chen J., Chen P., Chen Chia, Surface motion of multiple alluvial valleys for incident plane SH-waves by using a semi-analytical approach. *Soil Dyn. Earthq. Eng.* 2008; 28:58–72.
7. Lee V.W., Luo H., Liang J.. Antiplane (SH) waves diffraction by a semicircular cylindrical hill revisited: an improved analytic wave series solution. *J. Eng. Mech.* 2006; 132: 1106-1114.
8. Yuan X., Men F.. Scattering of plane SH waves by a semi-cylindrical hill. *Earthq. Eng. Struct. Dyn.* 1992;21: 1091-1098.
9. Todorovska M.I., Hayir A., Trifunac M.D.. Antiplane response of a dike on flexible embedded foundation to incident SH-waves. *Soil Dynamics and Earthquake Engineering.* 2001; 21: 593-601
10. Yuan X., Liao Z., Trifunac M.D.. Surface motion of a cylindrical hill of circular-arc cross-section for incident plane SH waves. *Soil Dyn. Earthq.Eng.* 1996; 15:189-199.
11. Tsaur D., Chang K.. An analytical approach for the scattering of SH waves by a symmetrical V-shaped canyon: shallow case. *Geophys. J. Int.* 2008;174:255-264.
12. Tsaur D., Chang K., Hsu M.. An analytical approach for the scattering of SH waves by a symmetrical V-shaped canyon: deep case. *Geophys. J.Int.* 2010; 183:1501-1511.
13. Zhang N., Gao Y., etal. Scattering of SH waves induced by a non-symmetrical V-shaped canyon, *Geophys. J. Int.* 2012; 191: 243-256.
14. Chang K., Tsaur D., Wang J.. Scattering of SH waves by a circular sectorial canyon. *Geophys. J. Int.* 2013;195:532-543.
15. Tsaur D., Chang K., Hsu M.. Ground motions around a deep semielliptic canyon with a horizontal edge subjected to incident plane SH waves. *J. Seismol.* 2018; 22:1579-1593

- 
16. Yang Z.L., et al. Scattering of SH waves by a non-symmetrical V-shaped canyon with a shallow cavity in half-space. *WAVE RANDOM COMPLEX* . 2021; 22:1745-5030
  17. Liang J.W., Luo H., Lee V.W.. Scattering of plane SH waves by a circular-arc hill with a circular tunnel. *Acta Seismologica Sinica(English Edition)*, 2004; 05: 41-55.
  18. Liu D. K. and Hu C.. Scattering of flexural wave and dynamic stress concentration in Mindlin thick plates. *Acta Mechanica Sinica*. 1996;12:169-185
  19. Zhou C.P., Ma F.. Dynamic stress concentrations in exponential graded materials with two holes of arbitrary shape. *Wave Motion*. 2014; 51(3): 466-475
  20. Hu C., Liu D.K.. Dynamic stress concentrations in thick plates with two holes based on refined theory. *Applied Mathematics and Mechanics (English Edition)*. 2014; 35(12): 1591-1606.
  21. Wang Q.Y., Chen D.H.. Elastic wave scattering and dynamic stress concentrations in stretching thick plates with two cutouts by using the refined dynamic theory. *Acta Mechanica Solida Sinica*. 2018; 31(3): 332-348.
  22. Qiu F.Q., Liu D.K. Antiplane Response of Isosceles Triangular Hill to Incident SH waves. *Earthquake Engineering and Engineering Vibration*. 2005: 4(1): 37-43.
  23. Lin S.Z., Qiu F.Q., Liu D.K.. Scattering of SH waves by a scalene triangular hill. *Earthquake Engineering and Engineering Vibration*. 2010.
  24. Yang Z.L., Song Y.Q., et al. Scattering of plane SH waves by an isosceles trapezoidal hill. *Wave Motion* 2019; 92: 102415-102415.
  25. Shyu W.-S., Teng T.-J.. Hybrid method combines transfinite interpolation with series expansion to simulate the anti-plane response of a surface irregularity. *Journal of Mechanics*. 2014; 4: 349-360
  26. Shyu W.-S., Teng T.-J.. Anti-plane response caused by interactions between a dike and the surrounding soil. *Soil Dyn. Earthq. Eng.* 2017; 92: 408-418,
  27. Martin P. A.. Scattering by a Cavity in an Exponentially Graded Half-Space. *Journal of Applied Mechanics*. 2009; 76(3):540-545.
  28. Hei B.P., Yang Z.L., et al. Modelling and analysis of the dynamic behavior of inhomogeneous continuum containing a circular inclusion. *Applied Mathematical Modelling*. 2015; 39: 7364-7374
  29. Ting T.C.T.. Existence of anti-plane shear surface waves in anisotropic elastic half-space with depth-dependent material properties. *Wave Motion*. 2010; 47: 350-357
  30. Achenbach, J. D. , and O. Balogun. Anti-plane surface waves on a half-space with depth-dependent properties, *Wave Motion* 2010; 47: 59-65.

- 
31. Shuvalov A.L., Poncelet O., Kiselev A.P.. Shear horizontal waves in transversely inhomogeneous plates. *Wave Motion*. 2008; 45: 605-615.
  32. Liu D.K.. Dynamic stress concentration around a circular cavity by SH wave in an anisotropic media. *Acta Mechanica Sinica*. 1988; 20(5): 443-452.
  33. Liu D.K., Han F.. Scattering of plane SH wave by canyon topography in anisotropic medium. *Earthquake Engineering and Engineering Dynamics*.1990; 10(2): 11-24.
  34. Liu D.K.,Yuan Y.C.. Far field displacement around a circular cavity caused by SH wave in an anisotropic medium. *Earthquake Engineering and Engineering Dynamics*. 1988; 8(1): 50-59. ( in Chinese)
  35. Liu D.K., Xu Y.Y.. Interaction of multiple semi-cylindrical canyons by plane SH wave in anisotropic media. *Acta Mechanica Sinica*. 1993; 25(1): 93-102 .
  36. Liu D.K., Han F. Scattering of plane SH wave by noncircular cavity in anisotropic media. *Journal of Applied Mechanics. Transactions ASME*. 1993; 60(3): 769-772.
  37. Chen Z.G.. Dynamic stress concentration around shallow cylindrical cavity by SH wave in anisotropically elastic half-space. *Rock and Soil Mechanics*. 2012; 33(3): 899-905.
  38. Yang Z.L., Jiang G.X.X., et al. The role of soil anisotropy on SH wave scattering by a lined circular elastic tunnel in an elastic half-space soil medium. *SOIL DYN EARTHQ ENG*, 2019; 125: 105721.1-105721.4.
  39. Jiang, G. , Yang, Z. , Sun, C. , Sun, B. , & Yang, Y. . Dynamic analysis of anisotropic half space containing an elliptical inclusion under SH waves. *Mathematical Methods in the Applied Sciences*. 2020;
  40. Tarinejad R., Isari M., Ghalesari A.T.. A new boundary element solution to evaluate the geometric effects of the canyon site on the displacement response spectrum. *Earthq Eng & Eng Vib*. 2019; 018(002): 267-284.
  41. Zhong W.F., Nie G.H.. The scattering of SH wave by numerous inhomogeneities in an anisotropic body. *Acta Mechanica Solida Sini-ca*. 1988; 9( 1): 1-14
  42. Zhong W.F., Qian W.P. A boundary element method for calculation the SH wave scattering from arbitrarily shaped holes in an aniso-tropic mediun. *Acta Mechanica Solida Sinica*. 1990; 11(4): 285-297
  43. Du X.L., Xiong J.G.. Propagation of SH wave in anisotropic midium and the solution by boundary element method. *Engineering Me-chanices*, 1989; 6(3): 10-18
  44. Vishwakarma S.K., Panigrahi T.R.. Dynamics of SV-wave, SH-wave, and P-wave in a cross-anisotropic medium exhibiting exponential heterogeneity. *Arabian Journal of Geosciences*. 2021; 14(5): 1-16.

- 
45. Zhan Q., Zhuang M., Fang Y., et al. Full-anisotropic poroelastic wave modeling: A discontinuous Galerkin algorithm with a generalized wave impedance. *Computer Methods in Applied Mechanics & Engineering*. 2019; 346(APR.1):288-311.
  46. Achenbach J.D.. Shear waves in an elastic wedge. *Solids and Structures*. 1970; 6: 379-388,